

RESEARCH ARTICLE

Regulation of intercellular TARGET OF MONOPTEROS 7 protein transport in the *Arabidopsis* root

Kuan-Ju Lu¹, Bert De Rybel^{1,2,3}, Hilda van Mourik¹ and Dolf Weijers^{1,*}

ABSTRACT

Intercellular communication coordinates hypophysis establishment in the *Arabidopsis* embryo. Previously, TARGET OF MONOPTEROS 7 (TMO7) was reported to be transported to the hypophysis, the founder cell of the root cap, and RNA suppression experiments implicated its function in embryonic root development. However, the protein properties and mechanisms mediating TMO7 protein transport, and the role the movement plays in development remained unclear. Here, we report that in the post-embryonic root, TMO7 and its close relatives are transported into the root cap through plasmodesmata in a sequence-dependent manner. We also show that nuclear residence is crucial for TMO7 transport, and postulate that modification, potentially phosphorylation, labels TMO7 for transport. Additionally, three novel CRISPR/Cas9-induced *tmo7* alleles confirmed a role in hypophysis division, but suggest complex redundancies with close relatives in root formation. Finally, we demonstrate that TMO7 transport is biologically meaningful, as local expression partially restores hypophysis division in a plasmodesmal protein transport mutant. Our study identifies motifs and amino acids that are pivotal for TMO7 protein transport, and establishes the importance of TMO7 in hypophysis and root development.

KEY WORDS: TMO7, Plasmodesmata, Cell-cell communication, Protein transport, Embryogenesis, RAM

INTRODUCTION

It has been known for some time that intercellular communication is vital for the development of multicellular organisms (Barlow and Carr, 1984; Bonner, 1998; Long et al., 2015; Niklas and Newman, 2013), for example to coordinate distant events or locally organize tissues (Balkunde et al., 2017; Corbesier et al., 2007; Kurata et al., 2005; Nakajima et al., 2001; Pi et al., 2015; Sessions et al., 2000; Tamaki et al., 2007; Yadav et al., 2011). Plant cell walls provide robust physical support to build elaborate tissues and structures; however, cell walls also prevent cell migration, and it is, therefore, important for plant cells to receive positional cues from their surroundings for proper development (Barlow and Carr, 1984; ten Hove et al., 2015; van den Berg et al., 1995, 1997). The development of plasmodesmata (PD), nano-channels connecting the two neighbouring cells, allows the direct transport of molecules


through cell walls, which can facilitate the adaptation to inner or outer cues (Lucas and Lee, 2004).

Many plant tissue patterning events have been shown to involve cell-cell communication (Bernhardt et al., 2005; Helariutta et al., 2000; Kim et al., 2003; Kurata et al., 2005; Rodriguez et al., 2016; Schlereth et al., 2010). One of the earliest of such events in plant ontogeny occurs during early embryogenesis in the flowering plant *Arabidopsis thaliana* (ten Hove et al., 2015). Formation of the embryonic root requires the transcription factor MONOPTEROS (MP; also known as AUXIN RESPONSE FACTOR 5 or ARF5), as *mp* mutants fail to form a root (Berleth and Jurgens, 1993; Hardtke and Berleth, 1998). The root forms from two cell populations: a set of embryonic cells and their extra-embryonic neighbour (the hypophysis) (Scheres et al., 1994). Both these cell populations develop abnormally in the *mp* mutant (Berleth and Jurgens, 1993; Hardtke and Berleth, 1998), but expression of MP exclusively in the embryonic cells complements not only the embryonic but also the hypophysis defect, indicating a non-cell-autonomous function (Weijers et al., 2006). The immobility of MP protein suggests the existence of downstream mobile signals (Weijers et al., 2006). A direct MP downstream target, TARGET OF MONOPTEROS 7 (TMO7), is transcribed in embryonic cells but the protein is found in the neighbouring hypophysis, strongly suggesting protein transport. Fusing TMO7 to triple GFP (3xGFP) prevented protein accumulation in the hypophysis, suggesting a size restriction to its movement (Schlereth et al., 2010). Based on RNA suppression approaches and local expression, TMO7 appears to contribute either to establishing hypophysis identity or to controlling its cell division plane (Rademacher et al., 2012; Schlereth et al., 2010). TMO7 is an atypical basic helix-loop-helix (bHLH) transcription factor that lacks the basic region and is significantly smaller than most mobile transcription factors studied to date. Key questions are how this protein is transported, what regulates the transport, and what role the movement plays in development.

Several transcription factors that control plant development have been shown to move between cells. The *Zea mays* *KNOTTED 1* gene (*KNI*), and its homologue in *Arabidopsis thaliana*, *SHOOT MERISTEMLESS* (*STM*), encode homeobox-domain (HD) proteins that help maintain the undifferentiated state of shoot apical meristem (SAM) cells (Kim et al., 2003; Long et al., 1996; Lucas et al., 1995; Vollbrecht et al., 1991). The *LEAFY* (*LFY*) protein, a helix-turn-helix transcription factor that also participates in SAM development, appears to move by diffusion (Sessions et al., 2000; Wu et al., 2003). In addition, *WUSCHEL* (*WUS*), another key HD-containing transcription factor that regulates and maintains SAM activity, was also reported to move through PD (Daum et al., 2014; Yadav et al., 2011). Likewise, in root development there are several known mobile transcription factors, of which the *SHORTROOT* protein has been studied in most detail. *SHORTROOT* (*SHR*), encoding a GRAS family transcription factor, is transcribed in stele tissues, but the *SHR* protein subsequently moves a layer outward to

¹Laboratory of Biochemistry, Wageningen University, Stippeneng 4, 6708 WE, Wageningen, The Netherlands. ²Ghent University, Department of Plant Biotechnology and Bioinformatics, Technologiepark 927, 9052 Ghent, Belgium. ³VIB Center for Plant Systems Biology, Technologiepark 927, 9052 Ghent, Belgium.

*Author for correspondence (dolf.weijers@wur.nl)

 K.-J.L., 0000-0002-3685-4732; B.D., 0000-0002-9551-042X; D.W., 0000-0003-4378-141X

the endodermis and quiescent centre (QC) cells where *SCARECROW* (*SCR*), encoding another protein in GRAS family, is expressed (Helariutta et al., 2000; Nakajima et al., 2001). Together with *SCR*, *SHR* regulates the expression of the C2H2 zinc-finger domain transcription factor genes *JACKDAW* (*JKD*) and *MAGPIE* (*MGP*) in the endodermis, which forms a feed-forward loop with *SCR* (Welch et al., 2007). *SHR* localizes in both cytoplasm and nucleus at stele; the interaction with *SCR*, *JKD* and *MGP* after movement, however, relocates the protein complex exclusively to the nucleus and prohibits the further movement of *SHR* (Gallagher et al., 2004; Nakajima et al., 2001; Welch et al., 2007). This transport regulation is crucial for proper pattern formation of roots, as ectopic expression of *SHR* by the ubiquitous 35S promoter alters cell fate and creates multiplication of cell layers in the root (Nakajima et al., 2001). Despite the importance of intercellular protein transport in general, the molecular mechanisms and intrinsic signals that control protein transport remain poorly understood.

To reveal protein transport mechanisms, efforts have focused on identifying the essential transport elements in mobile transcription factors. However, the protein domains that mediate transport of different proteins do not seem to have common features (Gallagher et al., 2014), and it is, therefore, unclear how mobile proteins are selected for transport. Currently, the accumulation and degradation of callose, a β -1,3-glucan, at the neck region of the PD aperture by callose synthase (*CalS*) and β -1,3-glucanase, respectively, is the most prominent mechanism regulating cell-cell communication (Burch-Smith and Zambryski, 2012; Gallagher et al., 2014; Guseman et al., 2010; Han et al., 2014; Levy et al., 2007; Vaten et al., 2011; Wu et al., 2016). A dominant *CalS* mutant, *cals3-2d*, was found to regulate the accumulation of callose in *Arabidopsis*. By constructing an inducible iCalSm system, the transport of *SHR* and its regulatory microRNA (miR165/166) was demonstrated to be blocked by the accumulation of callose at PD (Vaten et al., 2011). Yet, the accumulation of callose regulates the dilation of PD by physical closure and would not be expected to contribute to selectivity. The molecular mechanism of selective protein transport is still not well understood.

Here, we report that the *TMO7* protein moves through PD and that its movement contributes to hypophysis division. We show that *TMO7* protein mobility is shared with a small set of *TMO7*-like proteins. We further show that sequence, not protein size, determines mobility and we identified protein motifs that are crucial for subcellular localization and transport. Our study provides a framework for understanding the selective transport of transcription factors in the *Arabidopsis* root.

RESULTS

***TMO7* moves through plasmodesmata in the *Arabidopsis* root**

TMO7 is expressed in the early *Arabidopsis* embryo, is transported from the pro-embryo to the hypophysis, and RNA suppression interferes with embryonic root formation (Schlereth et al., 2010). However, expression levels are extremely low and immunofluorescence is required to visualize the *TMO7*-GFP fusion protein in the embryo. *TMO7* was originally identified as an MP/BDL-dependent gene in a transcriptome study on seedlings (Schlereth et al., 2010); we, therefore, addressed whether the post-embryonic root would represent a more accessible model for studying protein movement. We first observed the expression pattern of *pTMO7::n3GFP* (nucleus localization signal-triple GREEN FLUORESCENT PROTEIN), and compared it with *pTMO7::TMO7-GFP* and *pTMO7::TMO7-3GFP* in root tips

(Fig. 1, Schlereth et al., 2010). The *TMO7* promoter is expressed in meristematic and lateral root cap cells surrounding the QC and columella cells with a shootward-declining gradient. Although nearly absent, very weak expression can also be observed in columella cells (Fig. 1A,B). In *pTMO7::TMO7-GFP* plants, we observed strong fluorescent signals not only in cells with high promoter activity, but also in QC and columella cells (referred as columella cells hereafter), indicating the rootward movement of *TMO7-GFP* protein, consistent with the reported movement of *TMO7* in the *Arabidopsis* embryo (Fig. 1C; Schlereth et al., 2010). In contrast to *TMO7-GFP*, the expression of *TMO7-3GFP* is highly correlated with the *TMO7* promoter activity (Fig. 1B,D). Interestingly, the *TMO7-3GFP* protein seems to form aggregates in several cells, especially in cells above the QC (Fig. 1D). Also, the *TMO7-3GFP* protein is mostly excluded from the nucleus as low or no fluorescence signal was detected in the nucleus (Fig. 1D). The absence of fluorescence signal in columella cells indicates that movement of *TMO7-3GFP* is disrupted; however, weak GFP fluorescence was detected in cells below the QC in *pTMO7::TMO7-3GFP* roots (Fig. 1D, asterisk), which might be due to the weak expression of the *TMO7* promoter. To distinguish the weak activity of the *TMO7* promoter in columella cells from the signal derived from protein transport, the per-pixel fluorescence intensity ratio between columella cells and the rest of meristematic region was quantified (Fig. 1F, Fig. S1; see detailed description in Materials and Methods). Consistent with the qualitative observation, the fluorescence intensity in columella cells is $28.8 \pm 5.5\%$ (mean \pm s.d., $n=19$) of the fluorescence in the meristematic region in *pTMO7::n3GFP* lines. The ratios in *pTMO7::TMO7-GFP* and *pTMO7::TMO7-3GFP* are $76.9 \pm 9.6\%$ and $47.5 \pm 7.5\%$ ($n=19$ and 18 , mean \pm s.d.), respectively (Fig. 1F). These results indicate that the increase of fluorescence in columella cells in *pTMO7::TMO7-GFP* is due to the transport of *TMO7-GFP*, which is largely prevented in *pTMO7::TMO7-3GFP*. Importantly, these results show that, as in embryos, *TMO7* protein is mobile in the post-embryonic root, and that it involves similar constraints.

The finding that fusion to 3GFP impaired *TMO7* cell-to-cell transport (hereafter referred to as ‘*TMO7* transport’) suggests that *TMO7* might, like most other mobile TFs, migrate through PD, which have a size restriction (Otero et al., 2016). To investigate further the possible passage of *TMO7*, we observed the movement of *TMO7-GFP* in the *cals3-2d* mutant, which over-accumulates callose and prohibits transport via PD (Vaten et al., 2011). Consistent with the notion that *TMO7* moves through PD, the movement of *TMO7-GFP* was hampered in the primary root of *cals3-2d* mutants (Fig. 1E,F). Based on these observations, we conclude that *TMO7* protein moves through PD in the *Arabidopsis* root.

***TMO7* clade protein sequences instruct the unidirectional movement into root cap cells**

In sink tissues, like young leaves and apical meristem regions, small proteins (molecular weight lower than 50 kDa) can transport freely through PD by diffusion (Oparka et al., 1999). As *TMO7* is 93 amino acids (aa) long (~11 kDa), it might thus passively diffuse through PD. To investigate whether the movement is correlated with molecular weight, or rather a consequence of specific protein features, we focused on other small bHLH proteins. The *Arabidopsis* genome encodes four *TMO7*-like proteins (*TMO7L1-4*, also known as bHLH161, bHLH134, bHLH136 and bHLH166, respectively; De Rybel et al., 2011), all representing small bHLH TFs (92–94 aa; Fig. 2A,B). Within the *TMO7* clade, the amino acid

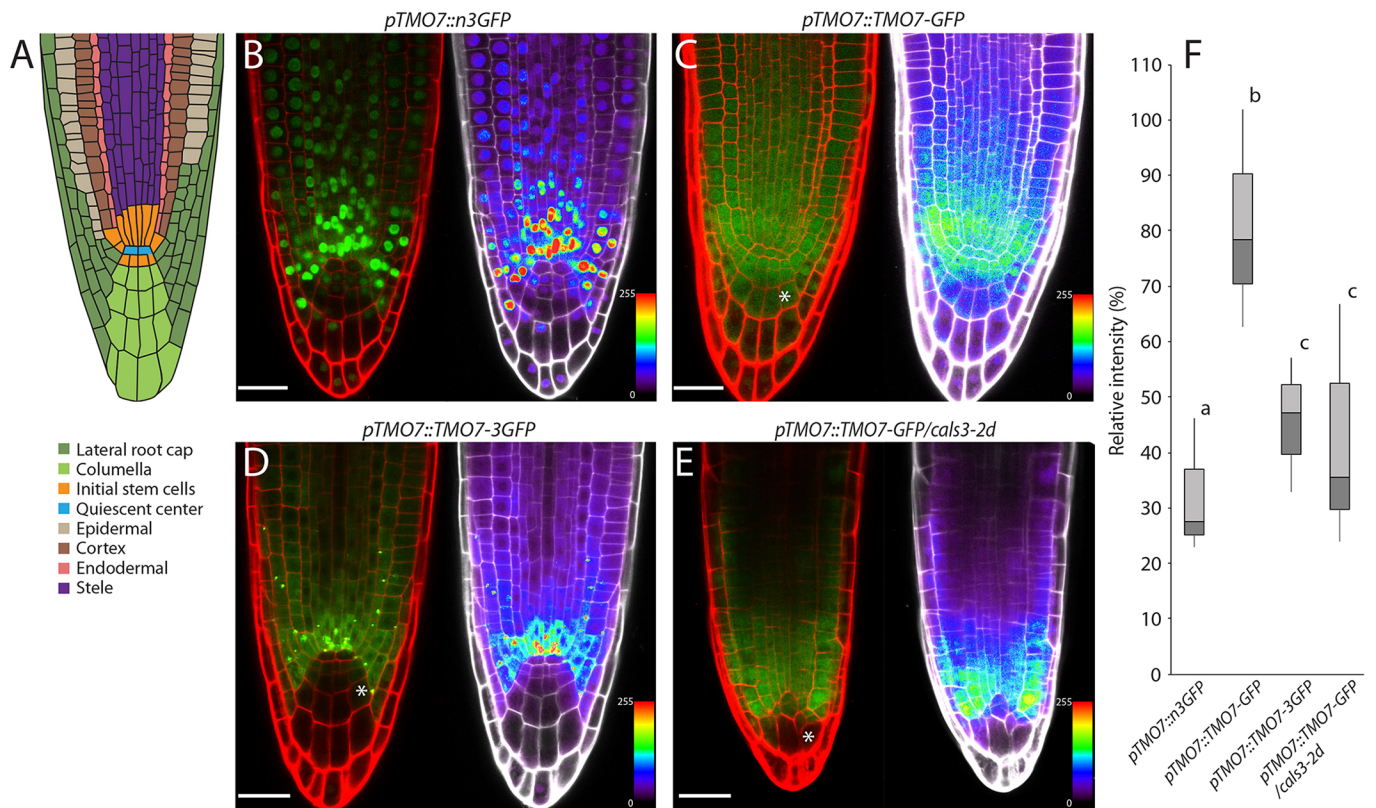


Fig. 1. TMO7 moves through plasmodesmata into root cap cells in the *Arabidopsis* primary root. (A) Schematic of *Arabidopsis* root structure. Different tissues are colour-coded as indicated in the key. (B-E) Five-day-old root fluorescence images in the median plane of pTMO7::n3GFP (B), pTMO7::TMO7-GFP (C), pTMO7::TMO7-3GFP (D) and pTMO7::TMO7-GFP in *cals3-2d* (E). Images on the left show GFP (green) and PI (red) fluorescence; false-colour images are shown on the right. (F) Statistical analysis of the fluorescence ratio between columella cell and stem cell niche regions of different transgenic plants. $n \geq 13$ roots per genotype, sample size is indicated in Materials and Methods. Significant differences ($P < 0.05$) as determined by one-way ANOVA with Tukey's post-hoc analysis are indicated by letters above bars. Asterisks mark the regions that show highest movement differences. Scale bars: 25 μm .

sequence is very conserved (up to 45% identity and 80% similarity; Fig. 2B). We therefore also selected two other small bHLHs outside the TMO7 clade, *AbHLH138* (AT2G31215, 129 aa, ~15 kDa) and *AbHLH151* (AT2G47270, 102 aa, ~12 kDa, also known as UPB1) (Fig. 2A,B), to uncouple size from homology. All small bHLH proteins were expressed as GFP fusion proteins from the *TMO7* promoter, and we visualized their localizations (Fig. 2C,D) and quantified their mobilities (Fig. 2E).

We observed comparable mobility of all proteins within the TMO7-like clade (Fig. 2D,E). The unrelated bHLH proteins *bHLH138* and *bHLH151* localize mainly to the nucleus (Fig. 2C), consistent with the presence of several basic residues (K, R; basic residues constitute nuclear localization signals) at the N terminal of the HLH domain (Fig. 2B). In addition, *bHLH138* also partially localized in the cytoplasm (Fig. 2C). Yet, despite their small size, the movement of *bHLH138*- or *bHLH151*-GFP is limited (Fig. 2C,E). Thus, we conclude that the transport of TMO7 clade proteins is not determined by their small protein size. Rather, the absence of a clear nuclear localization signal and/or the presence of conserved motifs within the TMO7 clade proteins might mediate transport through PD.

We further explored the transport at the root columella cells. We previously reported promoter activity of TMO7Ls: *bHLH134*, *bHLH136* and *bHLH166* are expressed weakly in the root cap and columella cells whereas *bHLH161* is expressed only in the lateral root cap (De Rybel et al., 2011). We therefore generated YFP fusion proteins with the endogenous promoters to explore the direction of

transport. Among these fusion proteins, the expression could only be detected for *bHLH134*-YFP (not shown) and *bHLH166*-YFP (Fig. 2F). Interestingly, both fusion proteins showed the highest intensity at the very tip of the columella cells with decreasing intensity toward the shoot, which is comparable to their promoter activity (Fig. 2F; De Rybel et al., 2011). Thus, we conclude that although *bHLH134* and *bHLH166* proteins are rootward mobile when expressed in the TMO7 expression domain, they do not normally move shootward from their expression site. This finding also suggests that the transport of TMO7-like proteins is unidirectional from the proximal to the distal meristem.

Protein sequence elements and subcellular localization define TMO7 transport

Given that the TMO7 protein sequence directs transport, we aimed to map the crucial region(s) by systematic mutation. We hypothesized that mutations that affect TMO7 mobility elements would disrupt transport. We performed a linker-scanning analysis by replacing regions of seven to nine amino acids with a poly-alanine linker of the same length and thus generated eleven TMO7 mutants (pTMO7::TMO7_{m1}-GFP to pTMO7::TMO7_{m11}-GFP; Fig. 3A). The relative intensity of fluorescence in the tip versus meristem was quantified in more than ten independent transgenic lines for each mutant (except for *m10*; only five T2 lines), and lines showed some variability in transport (Fig. 3C). Yet, the transport appeared to be unaffected in most mutant versions (Fig. 3B,C). We found a consistent reduction in the movement for two mutant

Fig. 2. TMO7 family proteins carry intrinsic features required for transport.

(A) Phylogenetic analysis of selected bHLH proteins in *Arabidopsis* based on the full-length protein sequence. Branch lengths indicate phylogenetic distances (scale bar indicates fraction of deviations). Green shading indicates the location of bHLH138 and bHLH151. Orange shading indicates TMO7 clade members. ARF5/MP is used as an unrelated reference. (B) Protein sequences comparison within the TMO7 family and between TMO7, bHLH138 and bHLH151. The schematic above indicates the location of the HLH domain and the mobile *cis*-elements in the TMO7 protein are shown in red. (C-E) Mobility analysis of bHLH138, bHLH151 and TMO7-like proteins. Confocal images of bHLH138-GFP and bHLH151-GFP (C); and bHLH134-, bHLH136-, bHLH161- and bHLH166-GFP expressed by the *TMO7* promoter (D) are shown as well as the fluorescence ratio analysis (E). Significant differences ($P < 0.05$), as determined by one-way ANOVA with Tukey's post-hoc analysis, are indicated by letters above bars. (F) Confocal images of *pbHLH166::3nGFP* and *pbHLH166::bHLH166-GFP*. Note that no fluorescence was detected outside the promoter active regions. Scale bars: 25 μ m.

proteins, *TMO7_{m5}* and *TMO7_{m8}*, similar to the pattern found in *pTMO7::n3GFP*, and *TMO7_{m9}* also consistently showed movement reduction, similar to *pTMO7::TMO7-3GFP* (Fig. 3B,C). In addition, *TMO7_{m2}*, *TMO7_{m3}* and *TMO7_{m4}* showed movement defects in some, but not all transgenic lines (Fig. 3B,C). We also observed that *TMO7_{m10}*-GFP intensity was slightly reduced in both meristem and tip region (Fig. 3B), and we asked whether reduction of the expression domain biased the intensity ratio in this case. We therefore selected a smaller (up to five cortex cells) meristematic region and compared intensity with the columella region. The comparison between *TMO7_{m6}*-GFP and *TMO7_{m10}*-GFP led to the same conclusion as the original statistics analysis (Fig. S1B), and

indicates that our quantitative analysis is robust to the selection of the region of interest. These results demonstrate that movement of TMO7 depends on at least two major and one minor elements.

By comparing the sequence between TMO7-like family proteins and the immobile bHLH138 and bHLH151 proteins, we found that the M5 region is located within the conserved HLH domain and is highly conserved between all TMO7 families. However, bHLH138 and bHLH151 have limited similarity within the M5 region (Fig. 2B). The M8/9 region is located immediately C terminal to the HLH domain, and this region is also highly conserved within the TMO7 family, but different in bHLH138 and bHLH151 (Fig. 2B). In addition, we also compared the bHLH domain of GLABRA 3 (bHLH1), a known mobile protein that regulates root hair formation (Bernhardt et al., 2005), with TMO7 and we only found limited similarity at the M5 or M8/9 regions (data not shown), indicating that tissue-specific transport systems might operate in the *Arabidopsis* root. These data suggest that the M5 and M8/9 regions could be specific elements responsible for the mobility of TMO7 family proteins.

An intuitive hypothesis would be that the *m5* and *m8/9* mutations alter the secondary or tertiary structure of the TMO7 protein and thus lead to movement defects. We analysed the possible secondary structure with the SWISS-MODEL protein-folding tool (<http://swissmodel.expasy.org/interactive>). The predicted TMO7 structure is very similar to the bHLH transcription factor MyoD (Fig. S2B; Ma et al., 1994); however, none of the mutants that disrupt movement is predicted to have a different secondary structure (Fig. S2A). It is therefore not directly evident how the mutations

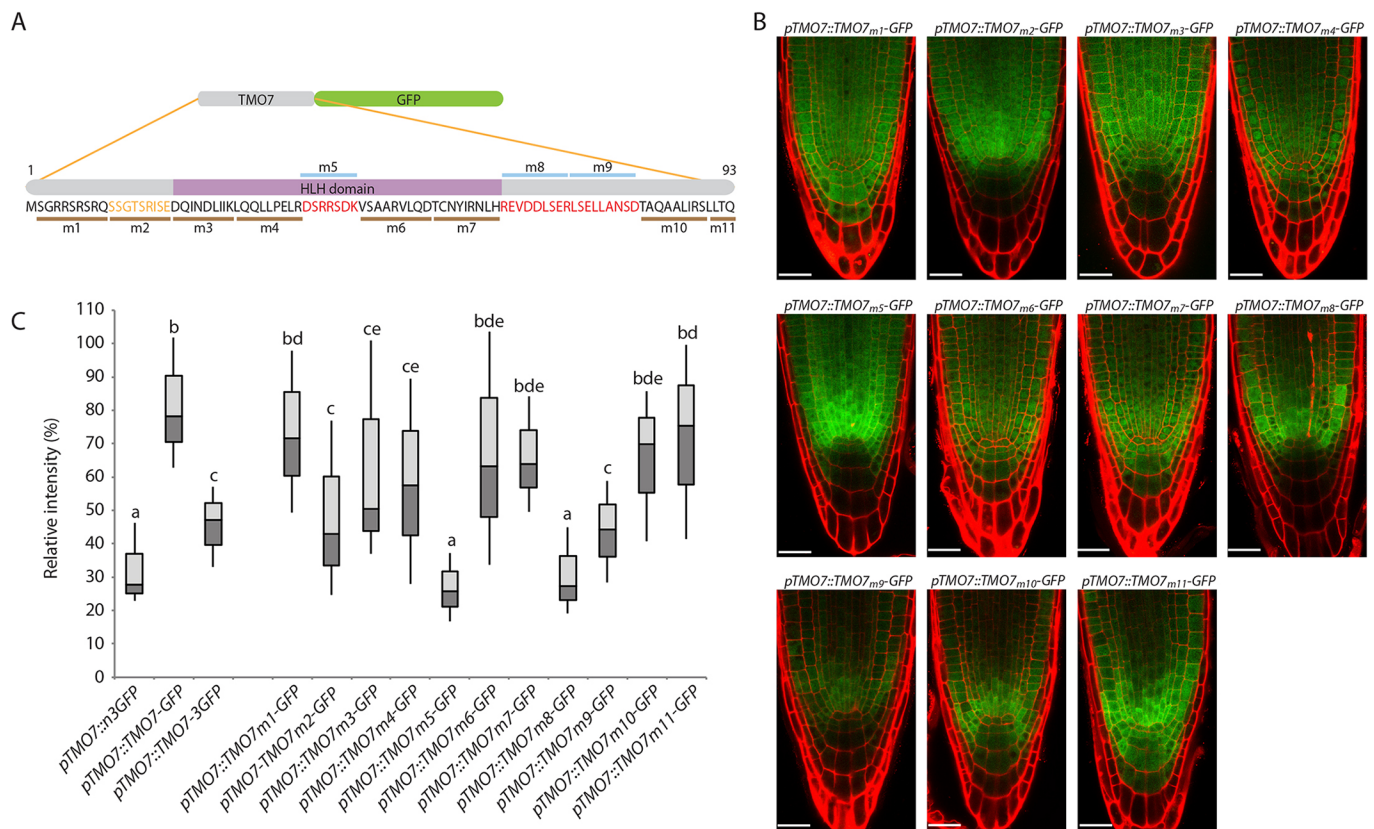


Fig. 3. TMO7 contains two major and one minor mobility motifs. (A) Schematic indicating the position of each mutant. Those indicated above the sequence are mobile defective mutants. (B) Confocal images of each linker-scanning mutant. Note that the QC and columella region in *m2*, *m5*, *m8* and *m9* regions show reduced or no fluorescence. (C) Fluorescence ratio analysis of linker-scanning mutants. Sample size is indicated in Materials and Methods. Significant differences ($P < 0.05$), as determined by one-way ANOVA with Tukey's post-hoc analysis, are indicated by letters above bars. Scale bars: 25 μ m.

would affect TMO7 protein properties, but given that no alternative secondary structures are predicted, the mutations might also not have dramatic consequences for protein folding.

To test further whether M5, M8 and M9 are bona fide mobility elements, sufficient for driving movement, we inserted these elements into bHLH138 and bHLH151 to create chimaeric proteins. Because the syntax surrounding M5 and M8/9 might also influence their function, chimaeric proteins were designed based on the syntax of TMO7. Based on the protein-folding prediction, M5 is localized at the loop region of the HLH domain (Fig. S2B). We directly inserted the TMO7 M5 sequence behind the loop region sequence of bHLH138 and replaced the loop sequence of bHLH151 with the TMO7 M5 sequence to create bHLH138-M5i and bHLH151-M5r. As there is no predicted secondary structure at the M8/9 region, and because it directly follows the HLH region in TMO7, we directly inserted the M8/9 region after the bHLH domain of bHLH138 and bHLH151 to generate bHLH138-M8/9 and bHLH151-M8/9, respectively. The combination of M5 and M8/9 was also constructed as bHLH138-M5i/8/9 and bHLH151-M5r/8/9 (Fig. 4). The direct insertion of M5 slightly improved the mobility of bHLH138 while the M8/9 region promoted the transport of bHLH151. All the other chimaeric bHLH138 and bHLH151 versions did not statistically improve movement (Fig. 4B). However, compared with TMO7, movement of chimaeric bHLH138-M5i and bHLH151-M89 was limited (Fig. 4B), perhaps owing to the strong nuclear localization of bHLH138 and bHLH151 (Fig. 2C, Fig. 4A).

It was previously shown that the movement of mobile proteins can be altered by localizing the protein to specific subcellular compartments (Crawford and Zambryski, 2000; Daum et al., 2014; Gallagher et al., 2004; Kim et al., 2005; Rodriguez et al., 2016; Tamaki et al., 2007). However, in contrast to a sole movement-restricting capacity of nuclear localization, in our linker-scanning analysis, we generally observed a lack of nuclear protein in movement-defective mutants (Fig. 3B, Fig. 5A). This suggests that transport into the nucleus might contribute to TMO7 transport. To test

whether strong subcellular localization interferes with the mobility of the protein, we generated TMO7-GFP protein with SV40 nucleus localization (NLS) or nuclear export signals (NES) at the N or C terminus of TMO7-GFP, respectively (NLS-TMO7-GFP; TMO7-GFP-NES). Like in other mobile proteins (Balkunde et al., 2017; Gallagher et al., 2004; Rodriguez et al., 2016), the nuclear localization signal restricted TMO7 movement. Surprisingly, however, the NES also hindered its mobility (Fig. 5B-D), plausibly by preventing the interaction of TMO7 with other factors that modify TMO7 as the export of TMO7 from nucleus seems to be efficient (Fig. 5C). These data suggest that entering as well as leaving the nucleus might be crucial for TMO7 transport.

In summary, the TMO7 family contains two major mobile *cis*-elements that are at least partially required for mobility of bHLH138 and bHLH151 when transplanted. However, the mobility strongly depends on subcellular localization; the strong NLS decreases the potential of direct interaction between TMO7 and PD, whereas the TMO7-GFP-NES result suggests that the import of TMO7 into the nucleus is also crucial for its movement.

Phosphorylation might control TMO7 mobility

Given that those specific motifs, as well as residence in the nucleus, seem to be important for TMO7 movement, we hypothesized that TMO7 transport involves post-translational modification. To start exploring this option, we first analysed the potential of phosphorylation on TMO7 using the DISPHOS tool, a phosphorylation prediction server (<http://www.dabi.temple.edu/disphos/>). Among the 19 serine, threonine and tyrosine residues, phosphorylation was predicted to occur on eight (Table S2). Among these, S39 and S42 are located within the M5 region (Fig. 3A). We therefore substituted each and both of the serine residues with alanine residues to create pTMO7::TMO7-S39A-, S42A- and S39, 42A-GFP, respectively. The subcellular localization of TMO7 was not altered by the mutations, indicating that protein import into the nucleus is not impaired by the mutation (Fig. 6A-C). Interestingly, however, all mutants showed impaired mobility (Fig. 6A-D), which

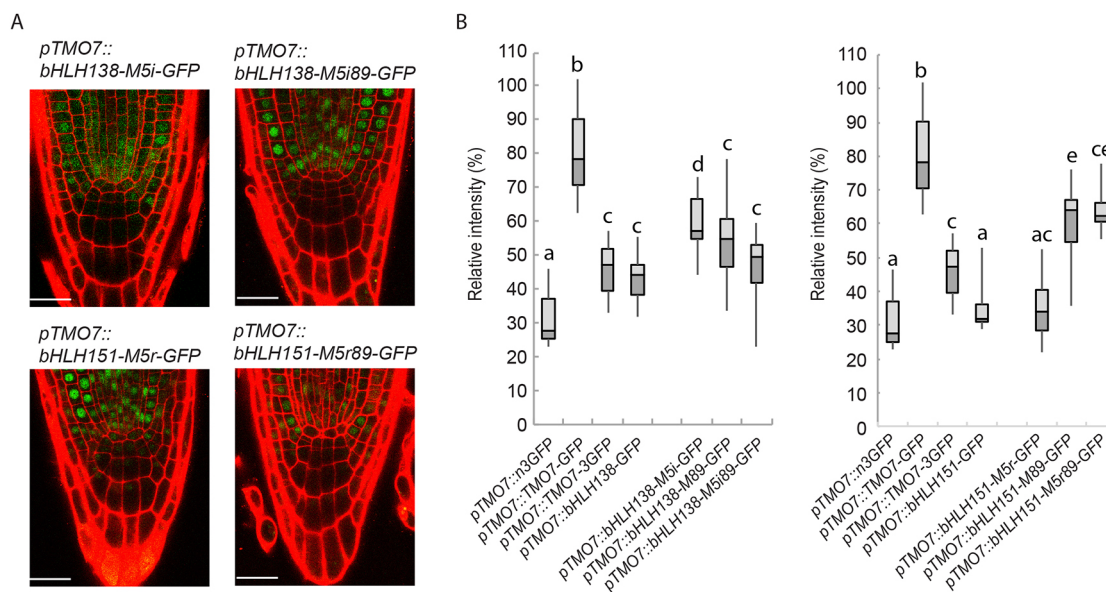


Fig. 4. Transferability of TMO7 mobility motifs. (A) Confocal images of bHLH138 and bHLH151 with M5 and M5, 8, 9 insertions. (B) Fluorescence intensity analysis of bHLH138-M5i, -M8,9, -M5i, 8, 9-GFP and bHLH151-M5r, -M8,9, -M5r, 8, 9-GFP. Sample size is indicated in Materials and Methods. Significant differences ($P < 0.05$), as determined by one-way ANOVA with Tukey's post-hoc analysis, are indicated by letters above bars. Note that the images have been enhanced for visualization. Scale bars: 25 μ m.

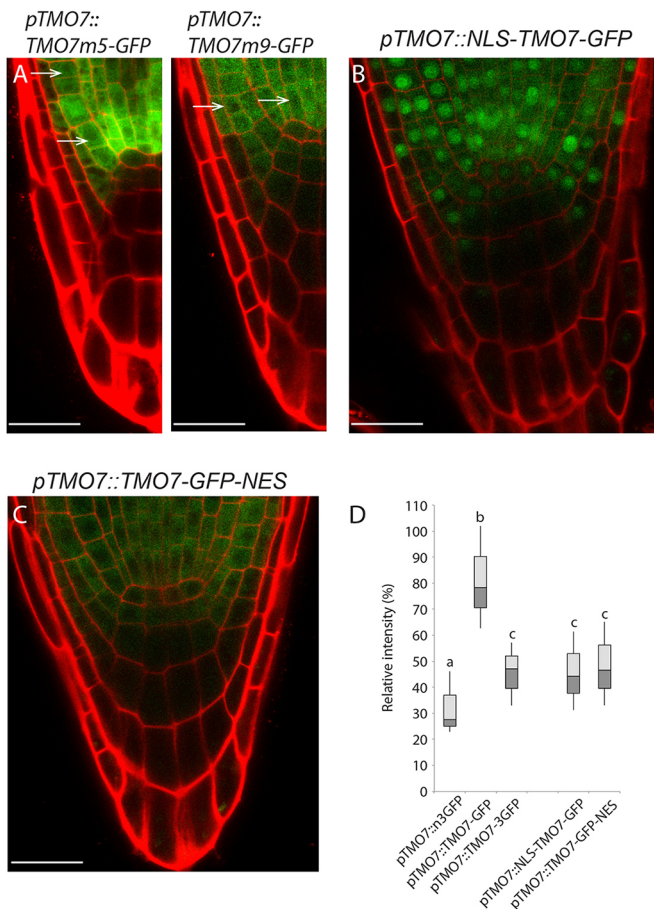


Fig. 5. Nuclear localization and exclusion signals restrict the movement of TMO7. (A) Confocal image of the *pTMO7::TMO7m5-GFP* and *pTMO7::TMO7m9-GFP* root tip. Arrows indicate nuclei without fluorescence. (B,C) Confocal images of *pTMO7::NLS-TMO7-GFP* (B) and *pTMO7::TMO7-GFP-NES* (C); note that fluorescence signal is absent in the root tip regions in both images. (D) Fluorescence intensity analysis of *pTMO7::NLS-TMO7-GFP* and *pTMO7::TMO7-GFP-NES*. Sample size is indicated in Materials and Methods. Significant differences ($P < 0.05$), as determined by one-way ANOVA with Tukey's post-hoc analysis, are indicated by letters above bars. Scale bars: 25 μ m.

suggests that both of these potential phosphorylation sites are important for TMO7 transport.

Characterization of a stable *tmo7* mutant reveals complex regulatory interactions

To address the importance of TMO7 transport, we first aimed to generate loss-of-function resources. Previously, we described a mild hypophysis division phenotype, as well as a low-penetrance rootless seedling defect in lines that had the *TMO7* gene silenced using RNAi or artificial microRNA expression. No phenotype could be observed in the available *tmo7-1* and *tmo7-2* insertion mutants (Schlereth et al., 2010). It is possible that RNAi and amiRNA (artificial microRNA) approaches targeted homologues as well as *TMO7*, or alternatively, it could be that the *tmo7-1* and *tmo7-2* insertion lines do not represent null alleles. Thus, we generated mutants through CRISPR/Cas9 gene editing (Tsutsui and Higashiyama, 2016). We designed a short guide RNA targeting the M5 mobile element and obtained three independent mutant alleles (*tmo7-4*, *tmo7-5* and *tmo7-6*), each creating shorter and mutated predicted proteins (Fig. 7A,B). In all CRISPR *tmo7* alleles,

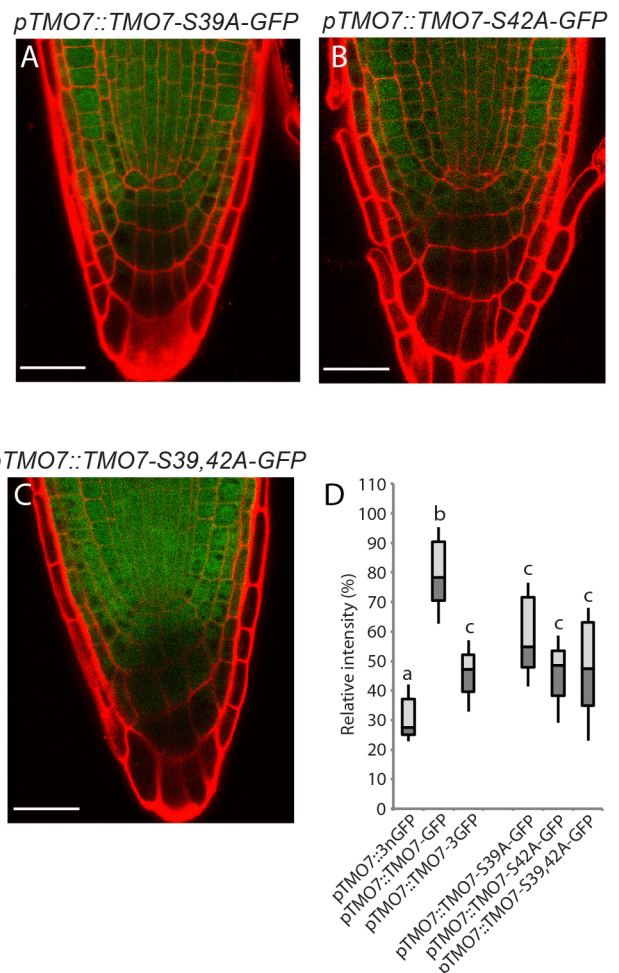


Fig. 6. Potential phosphorylation sites contribute to TMO7 movement. (A-C) Confocal images of *pTMO7::TMO7S39A-*, *S42A-*, and *S39, 42A-GFP*. (D) Fluorescence intensity analysis of *pTMO7::TMO7S39A-*, *S42A-*, and *S39, 42A-GFP*. Sample size is indicated in Materials and Methods. Note that the expression intensity of the TMO7 mutants is relatively low compared with the *pTMO7::TMO7-GFP* line; however, the statistical analysis still indicates the reduction of mobility in all the mutants. Note that the images were modified for visualization. Significant differences ($P < 0.05$), as determined by one-way ANOVA with Tukey's post-hoc analysis, are indicated by letters above bars. Scale bars: 25 μ m.

we observed that root length was reduced compared with wild-type plants (Fig. 7C,D and Table S3). In addition, we consistently found hypophysis division defects in all three mutant alleles (*tmo7-4*: 12.4%, $n=331$; *tmo7-5*: 5.6%, $n=302$; *tmo7-6*: 5%, $n=357$; Col: 1.8%, $n=277$; Fig. 7E). However, the rootless phenotype that was observed in 1-7% of seedlings in *amiRTMO7* and *TMO7* RNAi lines (Schlereth et al., 2010), was not recovered in the *tmo7-4*, *tmo7-5* and *tmo7-6* alleles ($n > 1000$ seedlings for *tmo7-4* and *tmo7-5*, $n > 600$ for *tmo7-6*). This suggests that the hypophysis defect might later be repaired by an as yet unknown mechanism in *tmo7-4*, *-5* and *-6* mutants.

One possibility is that the TMO7-like proteins act redundantly with TMO7; alternatively and additionally, *TMO7*-like genes might be involved in later stages and help generate an embryonic root following initial defects upon TMO7 depletion. In either scenario, it would be expected that the expression of *TMO7*-like genes is misregulated upon *TMO7* gene silencing, for example as an off-target effect. To test this possibility, we quantified TMO7L gene expression in primary roots of *TMO7* RNA suppression lines by

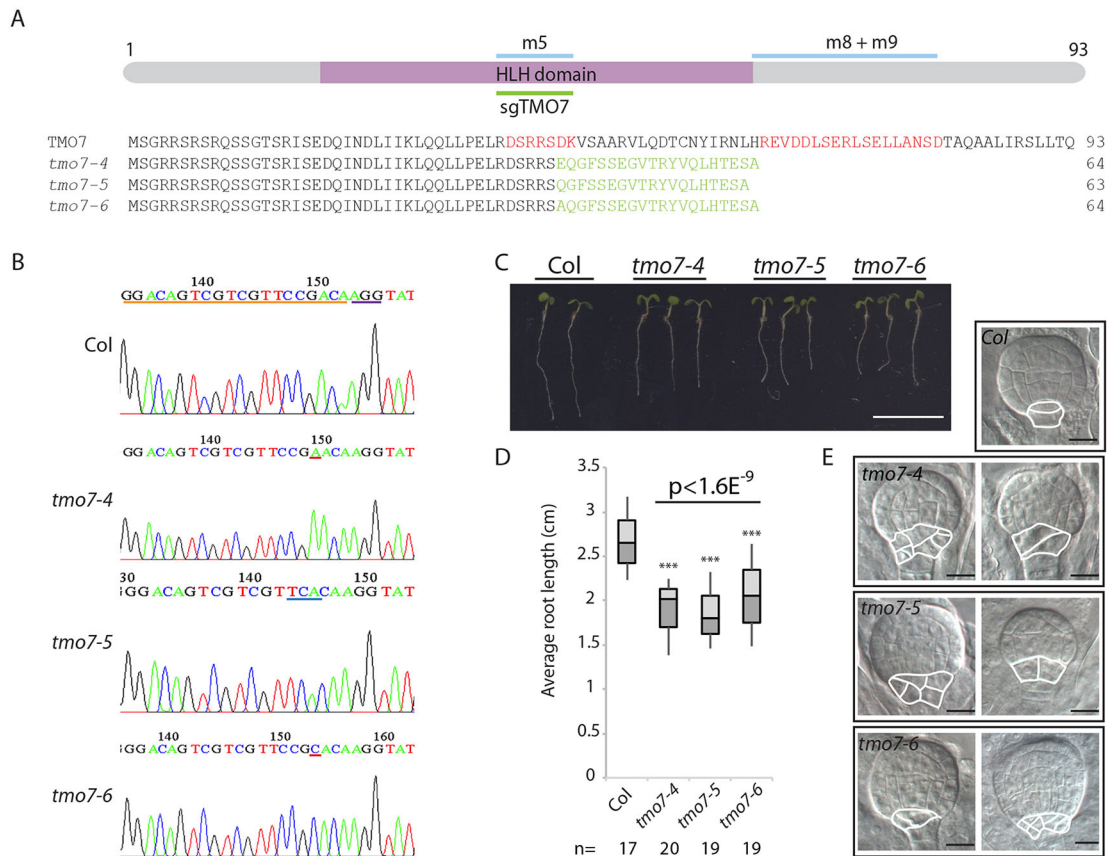


Fig. 7. Characterization of CRISPR/Cas9 *tmo7* mutants. (A) Schematic indicating the sgRNA targeting region and the mutated amino acid sequences (in green) of *tmo7-4*, *tmo7-5* and *tmo7-6*. (B) Sequencing traces of Col, *tmo7-4*, *tmo7-5* and *tmo7-6*. The orange underline indicates the sgRNA target sequence, the purple underline indicates the protospacer adjacent motif (PAM) in Col. The red underline indicates the inserted nucleotide in *tmo7-4* and *tmo7-6*, the blue underline indicates the deletion region in *tmo7-5*. (C) Root structure of Col, *tmo7-4*, *tmo7-5* and *tmo7-6*. Scale bar: 1 cm. (D) Average root length comparison between Col and CRISPR *tmo7* lines. *** $P < 0.01$ (Student's *t*-test). (E) DIC images of hypophysis division phenotype observed in *tmo7-4*, *tmo7-5* and *tmo7-6*. Scale bars: 10 μ m.

quantitative reverse transcription polymerase chain reaction (qRT-PCR). The results confirm that the *TMO7* transcript is downregulated between 15 and 70% in both *amiRTMO7* and *TMO7 RNAi* lines (Fig. S3A). Furthermore, we observed complex changes in the regulation of *TMO7* homologues, as different *TMO7*-like genes are downregulated in different gene silencing lines, whereas others are upregulated (Fig. S3A). In all *tmo7* CRISPR alleles, *TMO7* and all *TMO7*-like genes were expressed at a level comparable to wild type (Fig. S3B). These results are consistent with the notion that redundancy among *TMO7*-like genes might contribute to embryonic root formation. In RNA suppression lines, multiple homologues are affected, which could be the cause for the rootless phenotype. Clearly, a higher-order (CRISPR/Cas9) mutant, knocking out *TMO7*-like genes as well as *TMO7*, will be required to explore the function of *TMO7* in embryonic root formation.

TMO7 movement contributes to hypophysis division

To understand whether the movement of TMO7 is crucial for hypophysis development, we transformed the mobile *pTMO7::TMO7-GFP* and the immobile *pTMO7::TMO7-3GFP* into our CRISPR mutants and observed complementation of the hypophysis phenotype in T2 transgenic lines. We obtained ~5-8% hypophysis division defects in our CRISPR *tmo7* mutants, whereas in five independent *TMO7-GFP* transgenic lines, only 2% mutant

phenotypes were observed, similar to wild-type controls (Table S4). In contrast, in four independent *TMO7-3GFP* lines, we observed 5% of mutant phenotype in three lines, similar to the parental line, and in the other line, the mutant phenotype was similar to wild type (Table S4). As root length in the *tmo7-4*, *-5* and *-6* mutants is shorter than in wild type, we also quantified primary root length of all our transgenic lines. Similar to the complementation test in hypophysis, the *TMO7-GFP* transgenic lines mostly have longer root length than the parental lines (analysed with one-way ANOVA with Tukey's post-hoc, $P < 0.05$). In the *TMO7-3GFP* lines, the line that shows a wild type-like embryo phenotype also has significantly longer root than its parental lines whereas the remaining three lines are similar to their parental lines or in between the length of the parental lines and wild type (Fig. S4A). One explanation for the unexpected ability of non-mobile *TMO7-3GFP* protein to complement the *tmo7* mutant phenotype in this single transgenic line would be increased expression in the distal root meristem. Indeed, under the same imaging settings, we observed a relatively strong signal in the QC and columella cells of the complementing transgenic line, compared with the lines that do not complement the mutant phenotype (Fig. S4B). These results indicate that the mobile *TMO7-GFP* can rescue the *tmo7* phenotype whereas the immobile *TMO7-3GFP* cannot rescue the mutant phenotype unless it accumulates to high amounts in QC and columella cells.

Additionally, we employed the *cals3-2d* mutant to test further whether TMO7 mobility contributes to hypophysis development. The hyper-accumulation of callose in *cals3-2d* mutant prohibits the movement of macromolecules through PD, and we noticed that the mutant (Vaten et al., 2011) shows a strong rootless phenotype, resembling the *monopteros* (*mp*) (Berleth and Jurgens, 1993) and *TMO7*RNAi/*amiRTMO7* phenotypes (Fig. 8A). A detailed analysis of cell division patterns in the embryo showed a lack of hypophysis division in nearly all *cals3-2d* mutant embryos (Fig. 8C,D; 95%; $n > 700$ embryos). As auxin transport from embryo to hypophysis is essential for root formation (Friml et al., 2003; Weijers et al., 2006), we first tested whether the hypophysis and root defect in the *cals3-2d* mutant are related to an auxin accumulation problem. We transformed an auxin response reporter, *pDR5::nGFP*, (Weijers et al., 2006) into the *cals3-2d* background. The expression of *pDR5::nGFP* in the hypophysis was not affected by *cals3-2d* (Fig. 8B), which suggests that auxin is transported in a normal manner to the hypophysis in the mutant.

We next tested whether the expression of TMO7 in the cells to which it is normally transported (uppermost suspensor cells) would alleviate the division defect in the *cals3-2d* mutant. Therefore, TMO7 was expressed from the suspensor-specific *ARF13* promoter (Rademacher et al., 2012). By counting the correct division frequency of the hypophysis in both *pARF13::TMO7* and the *pDR5::nGFP* control, we found a partial rescue of hypophysis division in *cals3-2d* by *pARF13::TMO7* expression (Fig. 8E; $14.4 \pm 7.3\%$ with *pARF13::TMO7* compared with $6.0 \pm 1.5\%$ with *pDR5::nGFP*; $n = 7$ and 9 lines, respectively, with at least 90 individuals for each line; $P = 0.0126$ by two-tailed Student's *t*-test). We additionally also tested whether *pTMO7::TMO7-GFP* can rescue the phenotype. In this background, we observed a similar rate of normal divisions (about 1% in all transgenic lines) compared with *pDR5::nGFP* (Fig. 8E, Table S5). These results suggest that the hypophysis division phenotype in the *cals3-2d* mutant is probably caused by PD obstruction, which prevents TMO7 movement, but not auxin transport. Our findings thus indicate that TMO7 mobility contributes to the hypophysis division.

DISCUSSION

In this study, we systematically analysed the mobility of a specific small bHLH transcription factor protein family. We conclude that the transport of TMO7 is sequence dependent, but not primarily determined by protein size. Interestingly, the shuttling into and out of the nucleus appears to be crucial for mobility (Fig. 5). We postulate that this shuttling into the nucleus labels the protein for transport to other cells. The importance of nuclear localization for a mobile protein has also been proposed for the transport of SHR and another mobile R3-type MYB-like protein, CAPRICE (CPC), which is expressed in the non-hair epidermal cells in the roots and moves to the hair cells to specify the formation of the root hairs (Gallagher and Benfey, 2009; Gallagher et al., 2004; Kurata et al., 2005). A T289>I point mutation in SHR prevents the import of SHR into the nucleus and its intercellular transport and a W76A mutation of CPC largely reduced its nuclear localization and prevented its movement (Gallagher et al., 2004; Kurata et al., 2005). The tyrosine residue 289 of SHR was predicted to be a phosphor-acceptor that functions in dimerization and proper localization (Gallagher et al., 2004). Consistent with the role of T289 in SHR, the serine residues (S39 and S42) in TMO7 were also predicted to be phosphorylated. Replacing the residues with alanine hampers the intercellular movement, which suggests that phosphorylation might be a mark for intercellular transport (Fig. 6). However, we cannot rule out the possibility that these mutations act independently of phosphorylation by, for example, distorting the protein structure or preventing the interaction with an unknown factor that might be crucial for transport, but not for nuclear import. Further analysis of the post-translational modification status of mobile proteins is likely to provide more insight to intercellular communication mechanisms.

We previously showed that TMO7 is only transported into the hypophysis, but not into the upper tier of the pro-embryo (Schlereth et al., 2010). Consistent with this directional transport property in the embryo, we found that TMO7 family proteins can move from the root meristematic region into the root cap, but not in the opposite direction (Fig. 2D,F). In addition, in our *pTMO7::TMO7-3GFP* line, we observed obvious aggregations in the seedling root, which

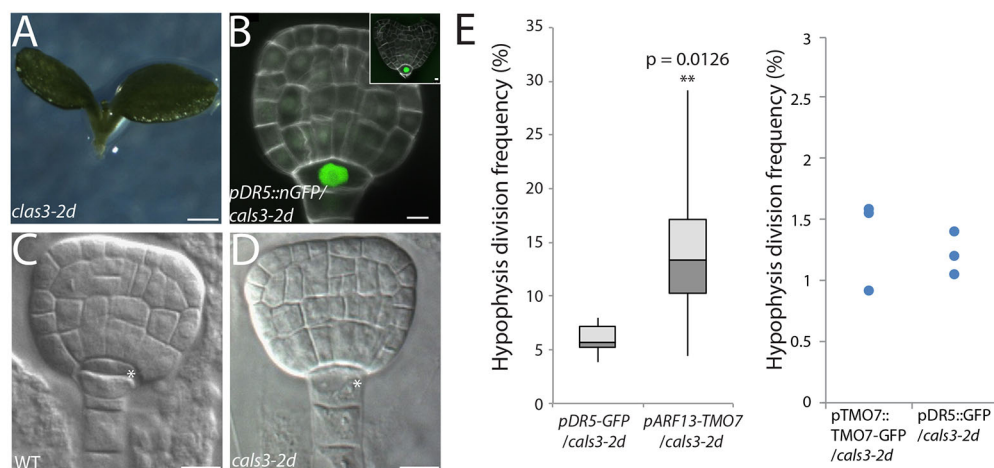


Fig. 8. Re-introduction of TMO7 into the *cals3-2d* suspensor partially complements the hypophysis division phenotype. (A) The rootless phenotype of the *cals3-2d* mutant. Scale bar: 100 μ m. (B) Expression of *pDR5::nGFP* in a *cals3-2d* embryo. Note that the accumulation of GFP signal is in the upper-most suspensor cell, and still no division has occurred in heart stage (inset). Scale bar: 5 μ m. (C,D) DIC image of a wild-type (WT) early-globular stage embryo (C) and a *Cals3-2d* late-globular stage embryo (D). Scale bars: 10 μ m. Note that the division that normally occurs in WT (asterisk in C) is absent in *cals3-2d* embryo (asterisk in D). (E) Left: Statistical analysis of wild-type division frequency in *pDR5::nGFP/cals3-2d* ($n = 7$ independent lines, at least 100 embryos per line) and *pARF13::TMO7/cals3-2d* ($n = 9$ independent lines, at least 90 embryos per line) embryos. $**P < 0.05$ (Student's *t*-test). Right: Independent analysis of *pDR5::nGFP* and *pTMO7::TMO7-GFP* in *cals3-2d*. $n = 3$ independent lines, at least 140 embryos per line.

were lacking in *pTMO7::TMO7-GFP* and other TMO7Ls-GFP fusion lines (Figs 1 and 2). The aggregations seem to be highly enriched in the meristematic cells closest to the neighbouring QC (Fig. 1D). It is possible that these clusters of proteins are TMO7 with intercellular transport markers but over the size limit for passing through PD. Interestingly, the stem cell maintenance transcription factor WUSCHEL HOMEBOX 5 (WOX5) has also been shown to move from the QC into the columella stem cells, and no shootward transport was observed (Pi et al., 2015). These data suggest that different regulatory mechanisms exist to control the rootward and shootward transport between root cap cells and other meristematic niche cells.

The cell walls between the pro-embryo and suspensor and between the upper and lower tiers in the embryo are generated by the very first and second cell divisions during embryogenesis (Scheres et al., 1994; ten Hove et al., 2015). The symplastic transport between suspensor and pro-embryo and within the pro-embryo was shown to be liberal until the globular stage, as soluble GFP moved from the suspensor to the whole embryo when expressed from the *SUC3* promoter and across the whole embryo when expressed from the *STM* promoter (Stadler et al., 2005). Interestingly, the shootward mobility of TMO7 to upper-tier cells is limited in the early embryo, which suggests that the symplastic transport control between the two tiers is established early in embryogenesis. How and why this control is established, and at which developmental stage is a very intriguing question.

In *tmo7-4*, *-5* and *-6*, we observed a clear hypophysis phenotype, which is consistent with the previous finding that TMO7 is involved in hypophysis development. Interestingly, however, no rootless phenotype was recovered. A possible scenario is that in the early embryo, TMO7 and other mobile factors coordinate the development of hypophysis whereas other TMO7 family genes control the later development of QC and root cap. This scenario could explain why hypophysis errors in *tmo7* CRISPR mutants do not lead to rootless defects. Indeed, both TMO7 gene silencing lines and *tmo7* CRISPR lines give rise to hypophysis defects but only the gene silencing lines show a low-frequency rootless phenotype, in which TMO7 family genes were misregulated (Fig. S4). It has been shown that the TMO7 family genes are not expressed at least until the late heart stage during embryogenesis but are expressed in the post-embryonic root in the columella and lateral root cap (De Rybel et al., 2011). Therefore, the misregulation of TMO7 family genes in RNA suppression lines might partially impair a redundancy-based repair mechanism. A higher-order TMO7 family mutant might reveal how TMO7 family genes help the development of hypophysis and post-embryonic root, and could also provide insight into the genes and cellular pathways that are controlled by mobile TMO7/TMO7L proteins in root formation and development.

MATERIALS AND METHODS

Plant materials

All seeds were surface sterilized, sown on half-strength MS (1/2MS) with 0.01% MES, 1% sucrose and 0.8% Daishin agar plates, and stratified for 1 day at 4°C in the dark before they were grown under long-day (16 h/8 h) conditions with a constant temperature of 22°C in a growth room. The TMO7 reporter lines *pTMO7::3nGFP*, *pTMO7::TMO7-GFP* and *pTMO7::TMO7-3GFP* have been previously described (Schlereth et al., 2010). The *cals3-2d* mutant (Vaten et al., 2011) was kindly provided by Ykä Helariutta (Sainsbury Laboratory Cambridge University, Cambridge, UK).

Cloning

All constructs except those for CRISPR/Cas9 gene editing were generated by ligation independent cloning (LIC) methods with pPLV02 vectors as previously described (De Rybel et al., 2011). For mobility analysis of

bHLH138/151, TMO7 family proteins, and TMO7 S39, 42A mutants, a vector containing the TMO7 promoter (*pTMO7* vector) was first created by amplification of a 2.2-kb promoter fragment from *pTMO7-n3GFP* that was subsequently ligated into the *EcoRI* and *BamHI* sites of the pPLV02 vector. The target genes and GFP were amplified separately with overlapping linkers and further fused by fusion PCR with primers containing the LIC adaptor. The TMO7 S39, 42A mutants were amplified using site-directed mutagenesis primers. The 5' and 3' fragments were further fused together by PCR primers containing the LIC adaptor. The fused fragments were integrated with the *pTMO7* vector by LIC. For alanine-linker scanning, the 2.2-kb promoter of TMO7 plus the 5' fragments before the mutation site and the 3' fragments after the mutation site plus the GFP tag were separately amplified by PCR. The two fragments were fused by PCR with primers containing the LIC site and further integrated with pPLV02 by LIC. All primers are listed in Table S1.

Microscopic and expression analysis

For imaging of roots, 5-day-old seedlings were incubated in 10 mg/ml propidium iodide (PI) solution for 1–2 min. GFP and PI were visualized by excitation at 488 nm and detection at 500–535 nm and 630–700 nm, respectively. For fluorescence ratio analysis, the two regions of interest (ROIs) were selected in the Leica Application Suite (LAS) program as in Fig. S1. The QC and three layers of columella cells were selected as ROI1; the lateral root cap cells and cells in the stem cell niche (up to the 12th cortex cell) were selected as ROI2. To prevent fluorescence intensity variation due to the tilting of the root, fluorescence of PI staining was used as the reference. The intensity ratio between the two channels of each individual ROI was first calculated, and the final intensity ratio was calculated by dividing the ratio of ROI1 by ROI2. For the movement analysis in the *cals3-2d* mutant, the ROIs were selected by morphology; besides the outer most root cap cells, three layers of cells near the root tip were selected as ROI1, and cells within five layers of epidermal cells were selected as the ROI2 region (Fig. S1). For imaging of embryos, ovules were isolated and mounted in a 4% paraformaldehyde/5% glycerol/PBS solution including 1.5% SCRI Renaissance Stain 2200 (R2200; Renaissance Chemicals) for counterstaining of embryos. After applying the coverslip, the embryos were squeezed out of the ovules, and R2200 and GFP fluorescence were visualized by excitation at 405 and 488 nm and detection at 430–470 and 500–535 nm, respectively. All confocal imaging was performed on a Leica SP5 II system equipped with hybrid detectors. For differential interference contrast (DIC) microscopy, dissected ovules were mounted in chloral hydrate solution (chloral hydrate, water and glycerol 8:3:1, w/v/v). After incubating overnight at 4°C, samples were investigated with a Leica DMR microscope equipped with DIC optics.

Phylogenetic and sequences comparison analysis

The phylogenetic relationships of selected bHLH family proteins were analysed by Clustal Omega (<http://www.ebi.ac.uk/Tools/msa/clustalo/>). The protein sequences were obtained from the TAIR website (<https://www.arabidopsis.org>) with the following AGI numbers: AT1G19850 (ARF5/MONOPTEROS), AT2G47270 (bHLH151/UPB1), AT3G25710 (bHLH32/TMO5), AT2G31215 (bHLH138), AT1G74500 (bHLH135/TMO7), AT2G41130 (bHLH106/TMO5L2), AT1G64625 (bHLH157), AT3G06590 (bHLH148/AIF2), AT2G43060 (bHLH158), AT1G68810 (bHLH30/TMO5L1), AT1G09250 (bHLH149/AIF4), AT3G28857 (bHLH166/TMO7L4), AT3G05800 (bHLH150/AIF1), AT3G47710 (bHLH161/TMO7L1), AT3G17100 (bHLH147/AIF3), AT2G31280 (bHLH155), AT5G39860 (bHLH136/TMO7L3) and AT3G56770 (bHLH107/TMO5L3).

Quantitative RT-PCR analysis

Total RNA of *Arabidopsis* seedling roots was extracted with the RNeasy kit (QIAGEN). Poly(dT) cDNA was prepared from 1 µg of total RNA with an iScript cDNA Synthesis Kit (Bio-Rad) and analysed on a CFX384 Real-Time PCR detection system (Bio-Rad) with iQ SYBR Green Supermix (Bio-Rad) according to the manufacturer's instructions. Primer pairs were designed with the Beacon Designer 7.0 (Premier Biosoft International). All individual reactions were performed in triplicate with three biological replicates. Data were analysed with qBase (Hellemans et al., 2007).

Expression levels were normalized to *ACTIN 2* (AT3G18780). The oligonucleotide sequences are listed in Table S1.

Statistical analysis

For relative intensity ratio comparison, we took confocal images from homozygous T3 lines (for *pTMO7::3nGFP*, *pTMO7::TMO7-GFP*, *pTMO7::TMO7-3GFP* and *pTMO7::TMO7-GFP/clas3-2d*, $n=19$, 19, 18 and 13 respectively), homozygous T2 lines [for TMO7-like: at least six independent lines and 18–25 images in total; for TMO7 linker-scanning mutants: at least ten independent lines and 15 images in total (except *m10* – five independent lines, 11 images); for NLS and NES analysis: at least six independent lines, 17 and 19 images; for TMO7-S39A and S42A, $n=6$ and 7 independent lines, and 13 and 16 images, respectively], and T1 lines (for bHLH138/151-GFP, $n=7$ and 13; bHLH138-M5i, -M89, -M5i89, $n=10$, 7 and 4; bHLH151-M5r, -M89, -M5r89, $n=10$, 15 and 4; for TMO7-S39, 42A, $n=7$ independent lines, respectively). Images were taken and the ROI1/ROI2 ratio was calculated as described above. The data were presented as box plots and analysed by one-way ANOVA with Tukey's post-hoc test ($P<0.05$). Note that we used the same *pTMO7::3nGFP*, *pTMO7::TMO7-GFP* and *pTMO7::TMO7-3GFP* data set as references in all figures and *pTMO7::bHLH138*- and *bHLH151-GFP* data sets in Fig. 4 as references for clarity.

For CRISPR *tmo7* mutant root length analysis, seedling images were taken by scanning 5 days after germinating on 1/2MS-agar plates. For complementation root length analysis, seedling images were taken by scanning 3 days after germinating on 1/2MS-agar plates. The root length was analysed using ImageJ (<https://imagej.net>). Student's *t*-test was used to analyse the significance for mutant root length analysis whereas one-way ANOVA with Tukey's post-hoc was used for complementation root length analysis.

CRISPR/Cas9 *tmo7* mutant generation

tmo7 CRISPR constructs were designed as previously described (Tsutsui and Higashiyama, 2016) with minor modifications. The short guidance RNA (sgRNA) sequence was designed in the reverse primer to amplify the U6 promoter and the forward primer to amplify the sgRNA scaffold. The two fragments were fused together using the sgRNA sequence as the overlapping region and amplified with primers with adaptor sequence complementary to the pKIR1.1 vector. The fused fragment was further integrated with the pKIR1.1 using the SLiCE cloning method (Zhang et al., 2014). After transformation, the red T1 *Arabidopsis* seeds were selected under the Leica M205 FA microscope equipped with epifluorescence. The T1 inflorescence apices were collected for genotyping (primers are listed in Table S1). The sequencing results were analysed using the web-tool TIDE (<https://tide.nki.nl>). The T2 generation of the transformants with high genome modification probability was harvested and non-fluorescent seeds were grown for genotyping analysis. Homozygous T3 were selected for embryonic and rootless phenotype analyses.

Acknowledgement

We thank Ykä Helariutta for generously sharing the *clas3-2d* mutant; Maritza van Dop, Colette ten Hove, Margo Smit, Prasad Vaddepalli and Jos Wendrich for constructive feedback on the manuscript; and members of the Weijers group for fruitful discussions.

Competing interests

The authors declare no competing or financial interests.

Author contributions

Conceptualization: K.-J.L., B.D.R., D.W.; Methodology: K.-J.L.; Validation: K.-J.L., B.D.R.; Formal analysis: K.-J.L., B.D.R., D.W.; Investigation: K.-J.L., B.D.R., H.v.M.; Resources: K.-J.L., B.D.R.; Writing - original draft: K.-J.L., D.W.; Writing - review & editing: K.-J.L., B.D.R., D.W.; Visualization: K.-J.L.; Supervision: B.D.R., D.W.; Project administration: D.W.; Funding acquisition: K.-J.L., B.D.R., D.W.

Funding

This work was supported by a fellowship from the Ministry of Science and Technology, Taiwan (103-2917-I-564-021 to K.-J.L.); by a grant from the European Research Council (ERC; StG CELLPATTERN; 281573 to D.W.); and by grants from

the Nederlandse Organisatie voor Wetenschappelijk Onderzoek (NWO; VIDI grant 842.06.012) and the Fonds Wetenschappelijk Onderzoek (FWO; Odysseus II G0D0515N to B.D.R.).

Supplementary information

Supplementary information available online at <http://dev.biologists.org/lookup/doi/10.1242/dev.152892.supplemental>

References

- Balkunde, R., Kitagawa, M., Xu, X. M., Wang, J. and Jackson, D. (2017). SHOOT MERISTEMLESS trafficking controls axillary meristem formation, meristem size and organ boundaries in Arabidopsis. *Plant J.* **90**, 435–446.
- Barlow, P. W. and Carr, D. J. (1984). *Positional Controls in Plant Development*. Cambridge Cambridge University Press.
- Berleth, T. and Jürgens, G. (1993). The role of the *monopteros* gene in organizing the basal body region of the Arabidopsis embryo. *Development* **118**, 575–587.
- Bernhardt, C., Zhao, M., Gonzalez, A., Lloyd, A. and Schiefelbein, J. (2005). The bHLH genes GL3 and EGL3 participate in an intercellular regulatory circuit that controls cell patterning in the Arabidopsis root epidermis. *Development* **132**, 291–298.
- Bonner, J. T. (1998). The origins of multicellularity. *Integr. Biol. Issues News Rev.* **1**, 27–36.
- Burch-Smith, T. M. and Zambryski, P. C. (2012). Plasmodesmata paradigm shift: regulation from without versus within. *Annu. Rev. Plant Biol.* **63**, 239–260.
- Corbesier, L., Vincent, C., Jang, S., Fornara, F., Fan, Q., Searle, I., Giakountis, A., Farrona, S., Gissot, L., Turnbull, C. et al. (2007). FT protein movement contributes to long-distance signaling in floral induction of Arabidopsis. *Science* **316**, 1030–1033.
- Crawford, K. M. and Zambryski, P. C. (2000). Subcellular localization determines the availability of non-targeted proteins to plasmodesmatal transport. *Curr. Biol.* **10**, 1032–1040.
- Daum, G., Medzihradsky, A., Suzuki, T. and Lohmann, J. U. (2014). A mechanistic framework for noncell autonomous stem cell induction in Arabidopsis. *Proc. Natl. Acad. Sci. USA* **111**, 14619–14624.
- De Rybel, B., van den Berg, W., Lokerse, A., Liao, C.-Y., van Mourik, H., Moller, B., Peris, C. L. and Weijers, D. (2011). A versatile set of ligation-independent cloning vectors for functional studies in plants. *Plant Physiol.* **156**, 1292–1299.
- Friml, J., Vieten, A., Sauer, M., Weijers, D., Schwarz, H., Hamann, T., Offringa, R. and Jürgens, G. (2003). Efflux-dependent auxin gradients establish the apical-basal axis of Arabidopsis. *Nature* **426**, 147–153.
- Gallagher, K. L. and Benfey, P. N. (2009). Both the conserved GRAS domain and nuclear localization are required for SHORT-ROOT movement. *Plant J.* **57**, 785–797.
- Gallagher, K. L., Paquette, A. J., Nakajima, K. and Benfey, P. N. (2004). Mechanisms regulating SHORT-ROOT intercellular movement. *Curr. Biol.* **14**, 1847–1851.
- Gallagher, K. L., Sozzani, R. and Lee, C.-M. (2014). Intercellular protein movement: deciphering the language of development. *Annu. Rev. Cell Dev. Biol.* **30**, 207–233.
- Guseman, J. M., Lee, J. S., Bogenschutz, N. L., Peterson, K. M., Virata, R. E., Xie, B., Kanaoka, M. M., Hong, Z. and Torii, K. U. (2010). Dysregulation of cell-to-cell connectivity and stomatal patterning by loss-of-function mutation in Arabidopsis *chorus* (glucan synthase-like 8). *Development* **137**, 1731–1741.
- Han, X., Hyun, T. K., Zhang, M., Kumar, R., Koh, E.-J., Kang, B.-H., Lucas, W. J. and Kim, J.-Y. (2014). Auxin-callose-mediated plasmodesmal gating is essential for tropic auxin gradient formation and signaling. *Dev. Cell* **28**, 132–146.
- Hardtke, C. S. and Berleth, T. (1998). The Arabidopsis gene *MONOPTEROS* encodes a transcription factor mediating embryo axis formation and vascular development. *EMBO J.* **17**, 1405–1411.
- Helariutta, Y., Fukaki, H., Wysocka-Diller, J., Nakajima, K., Jung, J., Sena, G., Hauser, M.-T. and Benfey, P. N. (2000). The SHORT-ROOT gene controls radial patterning of the Arabidopsis root through radial signaling. *Cell* **101**, 555–567.
- Hellemans, J., Mortier, G., De Paepe, A., Speleman, F. and Vandesompele, J. (2007). qBase relative quantification framework and software for management and automated analysis of real-time quantitative PCR data. *Genome Biol.* **8**, R19.
- Kim, J.-Y., Yuan, Z. and Jackson, D. (2003). Developmental regulation and significance of KNOX protein trafficking in Arabidopsis. *Development* **130**, 4351–4362.
- Kim, J.-Y., Rim, Y., Wang, J. and Jackson, D. (2005). A novel cell-to-cell trafficking assay indicates that the KNOX homeodomain is necessary and sufficient for intercellular protein and mRNA trafficking. *Genes Dev.* **19**, 788–793.
- Kurata, T., Ishida, T., Kawabata-Awai, C., Noguchi, M., Hattori, S., Sano, R., Nagasaka, R., Tominaga, R., Koshino-Kimura, Y., Kato, T. et al. (2005). Cell-to-cell movement of the CAPRICE protein in Arabidopsis root epidermal cell differentiation. *Development* **132**, 5387–5398.
- Levy, A., Erlanger, M., Rosenthal, M. and Epel, B. L. (2007). A plasmodesmata-associated beta-1,3-glucanase in Arabidopsis. *Plant J.* **49**, 669–682.

- Long, J. A., Moan, E. I., Medford, J. I. and Barton, M. K.** (1996). A member of the KNOTTED class of homeodomain proteins encoded by the STM gene of Arabidopsis. *Nature* **379**, 66-69.
- Long, Y., Scheres, B. and Blilou, I.** (2015). The logic of communication: roles for mobile transcription factors in plants. *J. Exp. Bot.* **66**, 1133-1144.
- Lucas, W. J. and Lee, J.-Y.** (2004). Plasmodesmata as a supracellular control network in plants. *Nat. Rev. Mol. Cell Biol.* **5**, 712.
- Lucas, W. J., Bouche-Pillon, S., Jackson, D. P., Nguyen, L., Baker, L., Ding, B. and Hake, S.** (1995). Selective trafficking of KNOTTED1 homeodomain protein and its mRNA through plasmodesmata. *Science* **270**, 1980-1983.
- Ma, P. C. M., Rould, M. A., Weintraub, H. and Pabo, C. O.** (1994). Crystal structure of MyoD bHLH domain-DNA complex: perspectives on DNA recognition and implications for transcriptional activation. *Cell* **77**, 451-459.
- Nakajima, K., Sena, G., Nawy, T. and Benfey, P. N.** (2001). Intercellular movement of the putative transcription factor SHR in root patterning. *Nature* **413**, 307-311.
- Niklas, K. J. and Newman, S. A.** (2013). The origins of multicellular organisms. *Evol. Dev.* **15**, 41-52.
- Oparka, K. J., Roberts, A. G., Boevink, P., Cruz, S. S., Roberts, I., Pradel, K. S., Imlau, A., Kotlizky, G., Sauer, N. and Epel, B.** (1999). Simple, but not branched, plasmodesmata allow the nonspecific trafficking of proteins in developing tobacco leaves. *Cell* **97**, 743-754.
- Otero, S., Helariutta, Y. and Benitez-Alfonso, Y.** (2016). Symplastic communication in organ formation and tissue patterning. *Curr. Opin. Plant Biol.* **29**, 21-28.
- Pi, L., Aichinger, E., van der Graaff, E., Llavata-Peris, C. I., Weijers, D., Hennig, L., Groot, E. and Laux, T.** (2015). Organizer-derived WOX5 signal maintains root columella stem cells through chromatin-mediated repression of CDF4 expression. *Dev. Cell* **33**, 576-588.
- Rademacher, E. H., Lokerse, A. S., Schlereth, A., Llavata-Peris, C. I., Bayer, M., Kientz, M., Freire Rios, A., Borst, J. W., Lukowitz, W., Jürgens, G. et al.** (2012). Different auxin response machineries control distinct cell fates in the early plant embryo. *Dev. Cell* **22**, 211-222.
- Rodriguez, K., Perales, M., Snipes, S., Yadav, R. K., Diaz-Mendoza, M. and Reddy, G. V.** (2016). DNA-dependent homodimerization, sub-cellular partitioning, and protein destabilization control WUSCHEL levels and spatial patterning. *Proc. Natl. Acad. Sci. USA* **113**, E6307-E6315.
- Scheres, B., Wolkenfelt, H., Willemsen, V., Terlou, M., Lawson, E., Dean, C. and Weisbeek, P.** (1994). Embryonic origin of the Arabidopsis primary root and root-meristem initials. *Development* **120**, 2475-2487.
- Schlereth, A., Möller, B., Liu, W., Kientz, M., Flipse, J., Rademacher, E. H., Schmid, M., Jürgens, G. and Weijers, D.** (2010). MONOPTEROS controls embryonic root initiation by regulating a mobile transcription factor. *Nature* **464**, 913-916.
- Sessions, A., Yanofsky, M. F. and Weigel, D.** (2000). Cell-cell signaling and movement by the floral transcription factors LEAFY and APETALA1. *Science* **289**, 779-782.
- Stadler, R., Lauterbach, C. and Sauer, N.** (2005). Cell-to-cell movement of green fluorescent protein reveals post-phloem transport in the outer integument and identifies symplastic domains in Arabidopsis seeds and embryos. *Plant Physiol.* **139**, 701-712.
- Tamaki, S., Matsuo, S., Wong, H. L., Yokoi, S. and Shimamoto, K.** (2007). Hd3a protein is a mobile flowering signal in rice. *Science* **316**, 1033-1036.
- ten Hove, C. A., Lu, K.-J. and Weijers, D.** (2015). Building a plant: cell fate specification in the early Arabidopsis embryo. *Development* **142**, 420-430.
- Tsutsui, H. and Higashiyama, T.** (2016). pKAMA-ITACHI vectors for highly efficient CRISPR/Cas9-mediated gene knockout in Arabidopsis thaliana. *Plant Cell Physiol.* **58**, 46-56.
- van den Berg, C., Willemsen, V., Hage, W., Weisbeek, P. and Scheres, B.** (1995). Cell fate in the Arabidopsis root meristem determined by directional signalling. *Nature* **378**, 62-65.
- van den Berg, C., Willemsen, V., Hendriks, G., Weisbeek, P. and Scheres, B.** (1997). Short-range control of cell differentiation in the Arabidopsis root meristem. *Nature* **390**, 287-289.
- Vaten, A., Dettmer, J., Wu, S., Stierhof, Y.-D., Miyashima, S., Yadav, S. R., Roberts, C. J., Campilho, A., Bulone, V., Lichtenberger, R. et al.** (2011). Callose biosynthesis regulates symplastic trafficking during root development. *Dev. Cell* **21**, 1144-1155.
- Vollbrecht, E., Veit, B., Sinha, N. and Hake, S.** (1991). The developmental gene Knotted-1 is a member of a maize homeobox gene family. *Nature* **350**, 241-243.
- Weijers, D., Schlereth, A., Ehrismann, J. S., Schwank, G., Kientz, M. and Jürgens, G.** (2006). Auxin triggers transient local signaling for cell specification in Arabidopsis embryogenesis. *Dev. Cell* **10**, 265-270.
- Welch, D., Hassan, H., Blilou, I., Immink, R., Heidstra, R. and Scheres, B.** (2007). Arabidopsis JACKDAW and MAGPIE zinc finger proteins delimit asymmetric cell division and stabilize tissue boundaries by restricting SHORT-ROOT action. *Genes Dev.* **21**, 2196-2204.
- Wu, X., Dinneny, J. R., Crawford, K. M., Rhee, Y., Citovsky, V., Zambryski, P. C. and Weigel, D.** (2003). Modes of intercellular transcription factor movement in the Arabidopsis apex. *Development* **130**, 3735-3745.
- Wu, S., O'Lexy, R., Xu, M., Sang, Y., Chen, X., Yu, Q. and Gallagher, K. L.** (2016). Symplastic signaling instructs cell division, cell expansion, and cell polarity in the ground tissue of Arabidopsis thaliana roots. *Proc. Natl. Acad. Sci. USA* **113**, 11621-11626.
- Yadav, R. K., Perales, M., Gruel, J., Girke, T., Jonsson, H. and Reddy, G. V.** (2011). WUSCHEL protein movement mediates stem cell homeostasis in the Arabidopsis shoot apex. *Genes Dev.* **25**, 2025-2030.
- Zhang, Y., Werling, U. and Edlmann, W.** (2014). Seamless ligation cloning extract (SLiCE) cloning method. *Methods Mol. Biol.* **1116**, 235-244.

Fig S1. Lu et al.

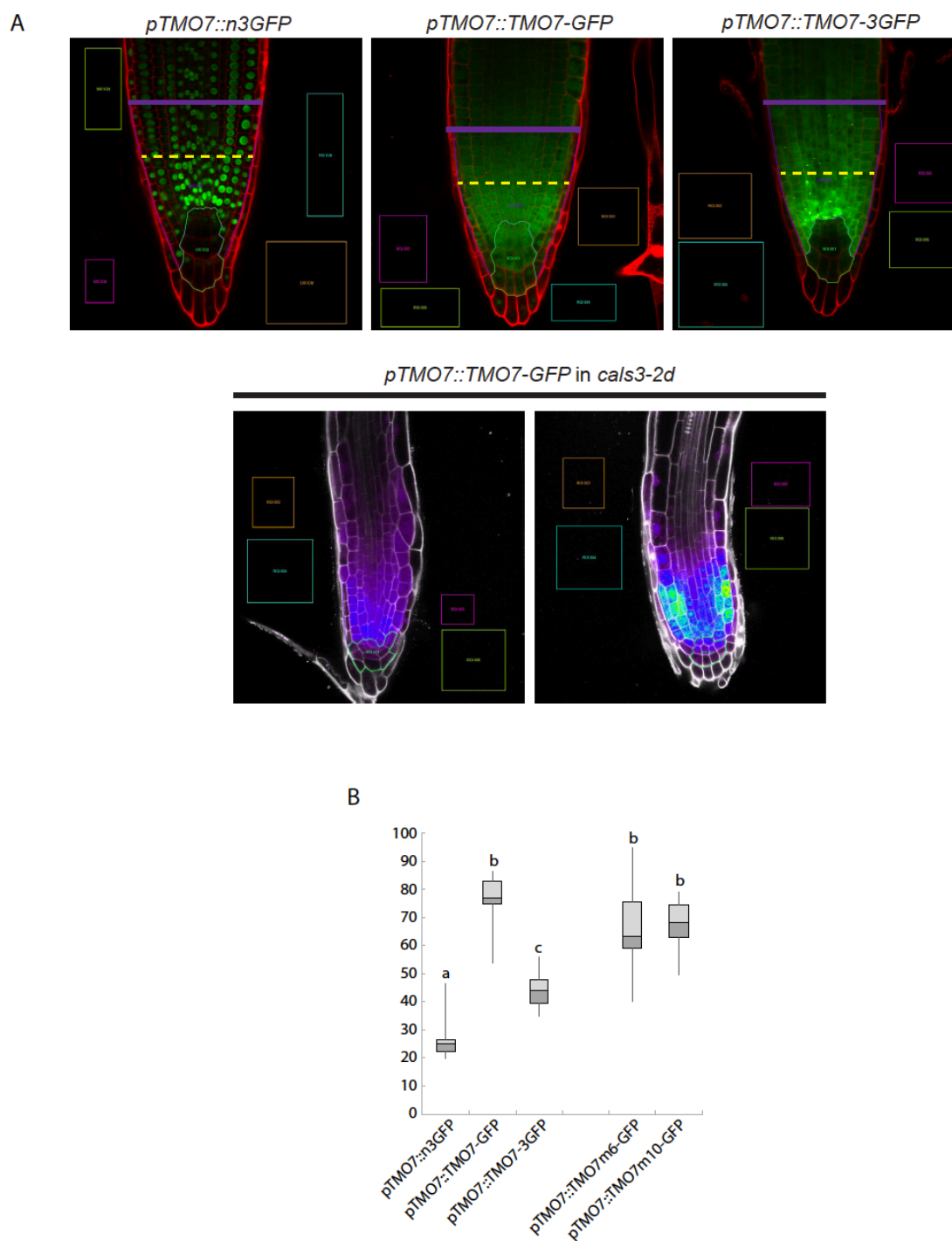


Fig S1. Sampling of Regions Of Interest (ROI) for statistical analysis. (A) Examples of confocal images analysed by the Leica Application Suite (LAS) program. The ROI1 (green region) was selected including the QC, and four layers of root cap cells. Regions outside the ROI1 up to the 12th cortex cell (indicated by the purple lines), besides the outer most root cap cells, were selected as the ROI2. Four other ROIs (ROI3-6) were selected to check the

background intensity. For selection in *cals3-2d*, the ROI1 and ROI2 were selected based on the morphology, the ROI1 includes 3 layers of cells from most distal region of the tip (excluding the most outer root cap cell), while ROI2 was selected based on the hypothetical cortex cells. (B) Intensity ratio of selected transgenic lines from Fig. 3 with narrower ROI2 region (indicated by the yellow dash lines). The results indicate that both TMO7_{m6}- and TMO7_{m10}-GFP have similar protein mobility to the TMO7-GFP.

Fig S2. Lu et al.

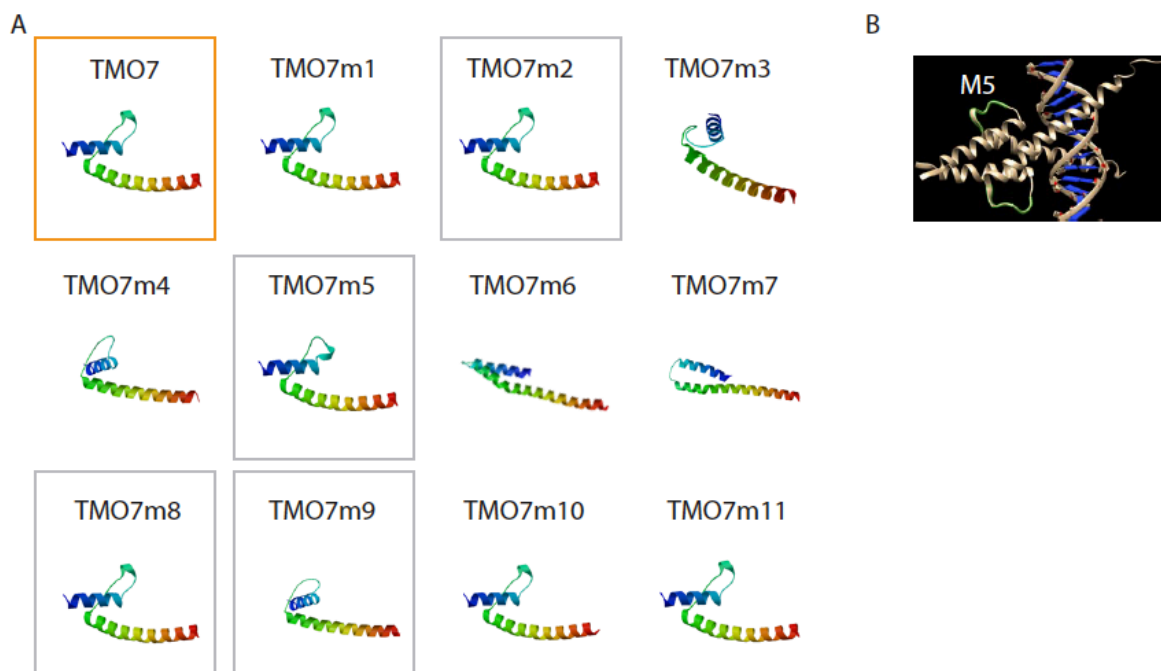


Fig S2. Structural homology models of TMO7 linker-scanning mutants. (A) The predicted structures of TMO7 and TMO7 mutants. The orange rectangle indicates the predicted TMO7 structure; Grey rectangles indicates the mutants affecting mobility. Note that only m9 has a minor predicted effect on structure while the remaining mobility mutants have the same predicted structure as TMO7. (B) The overlay of TMO7-M5 region on protein model of MyoD bHLH domain by chimera program (<https://www.cgl.ucsf.edu/chimera/>) with the PDB ID: 1MDY.

Fig S3 Lu et al.

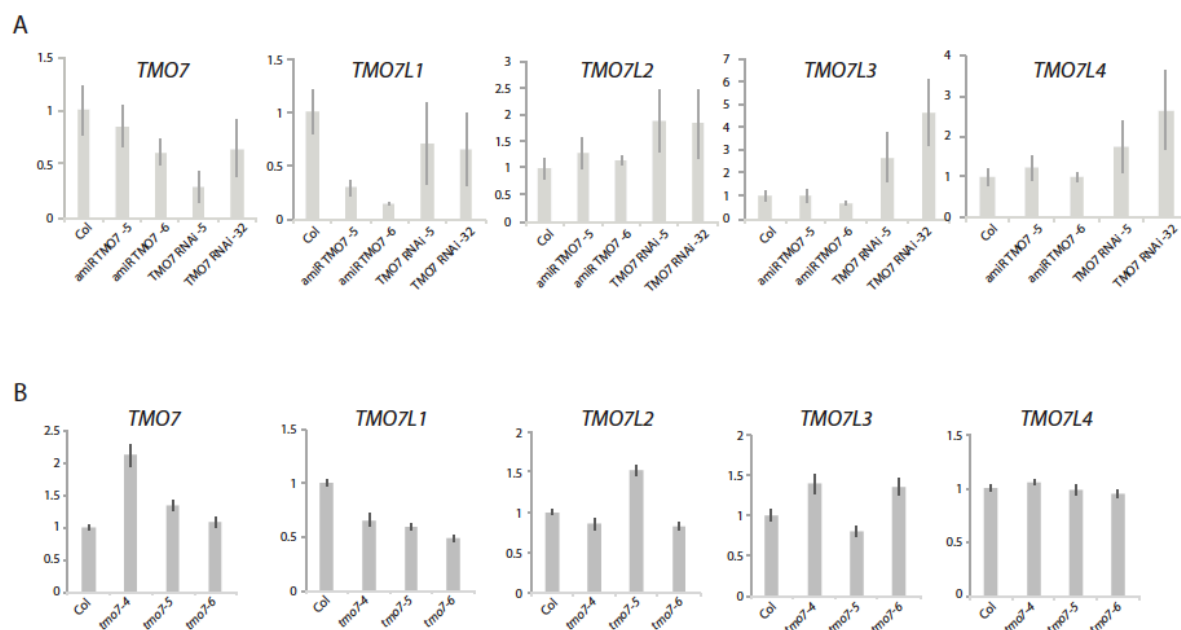


Fig. S3. Quantification of TMO7-Like genes in gene silencing lines and CRISPR/Cas9 generated *tmo7* mutants.

Expression level of *TMO7* family genes in (A) RNA suppression lines and (B) CRISPR/Cas9 *tmo7* lines by qRT-PCR analysis, relative expression level compared with endogenous control, *ACTIN2*. Note that in gene silencing lines, the *TMO7* family genes are highly interfered, while in CRISPR/Cas9 *tmo7* mutants, the gene expression is relatively stable. Quantified with three biological repeats and error bar indicates standard error of the mean.

Fig S4. Lu et al.

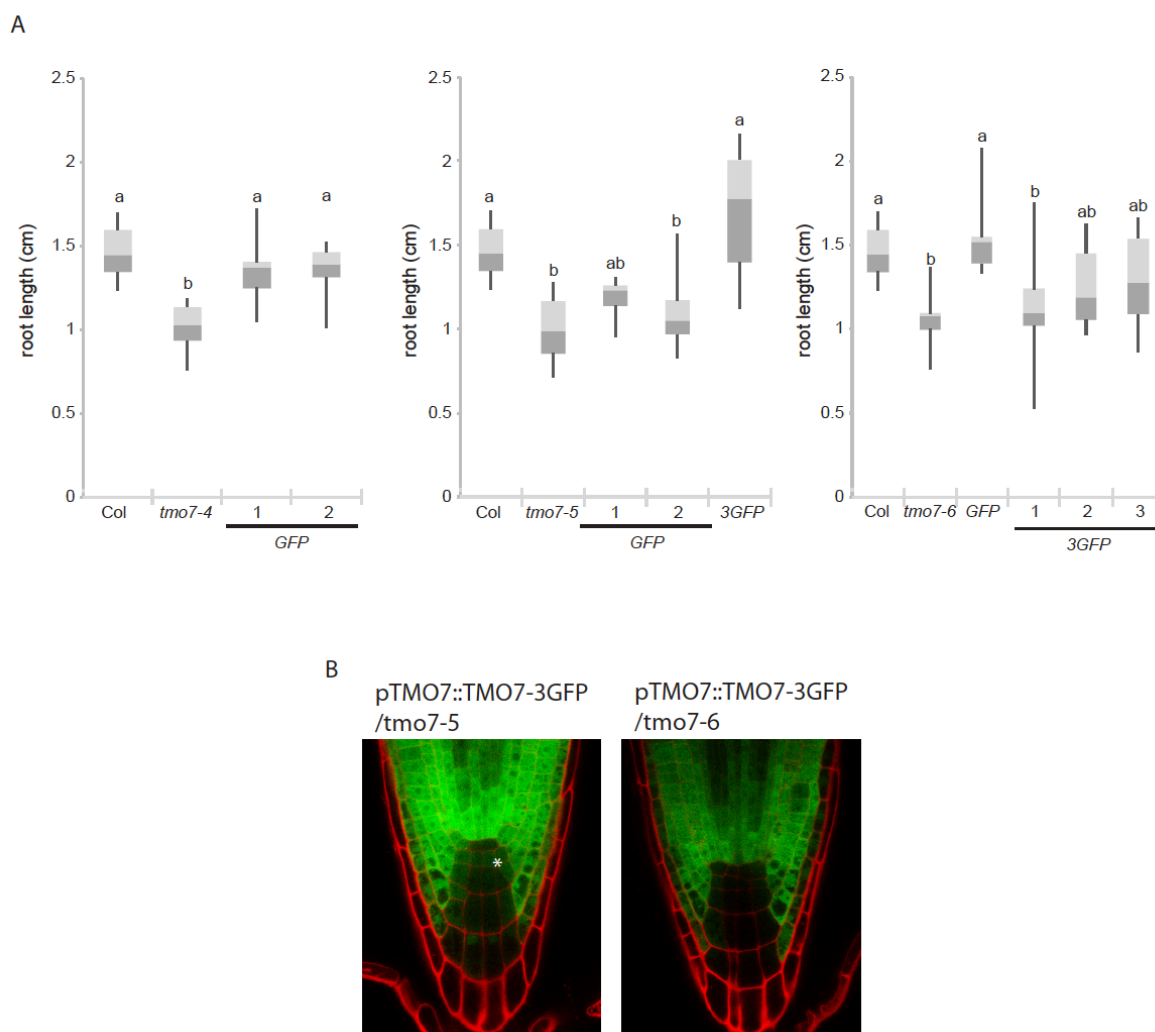


Fig S4. *tmo7* root complementation analysis and confocal images. (A) Box plot of 5-day-old seedling root length in different mutant background. Significant differences ($p < 0.05$), as determined by one-way ANOVA with Tukey's post-hoc analysis, are indicated by letters above bars. (B) Confocal images of pTMO7::TMO7-3GFP in *tmo7-5* (fully complement) and *tmo7-6* (no complementation) under the same confocal settings. Note that the expression level in the QC and columella cells in *tmo7-5* (indicated by the *) is higher than that in *tmo7-6*.

Table S1. List of oligo-nucleotides used in this research.

Name	Discription	Sequence	discription
KJ001	KJ LIC-TMO7 ^{pro} F	TAGTTGGAATAGGTTCTCGAGGTAGTTTCACTTT	forward primer for amplifying alenine linker mutant
KJ002	KJ TMO7 M1 N-term R	GGCAGCTGCGGCCGCGGCAGCCGCTGCCATTTTTTTGT AGAATATTG	reverse primer for 5' fragement of m1 mutant
KJ003	KJ TMO7 M2 N-term R	GGCAGCTGCGGCCGCGGCAGCCGCTGCTTGCCTCGAA CGTGATCTTC	reverse primer for 5' fragement of m2 mutant
KJ004	KJ TMO7 M3 N-term R	GGCAGCTGCGGCCGCGGCAGCCGCTGCTTCTGAGATC CTTGAAGTTC	reverse primer for 5' fragement of m3 mutant
KJ005	KJ TMO7 M4 N-term R	GGCAGCTGCGGCCGCGGCAGCCGCTGCCTTGATAATC AGATCATTTGA	reverse primer for 5' fragement of m4 mutant
KJ006	KJ TMO7 M5 N-term R	AGCTGCGGCCGCGGCAGCCGCCCTGAGCTCAGGAAGA AGCT	reverse primer for 5' fragement of m5 mutant
KJ007	KJ TMO7 M6 N-term R	GGCAGCTGCGGCCGCGGCAGCCGCTGCTGTCAATAT GTATCATGTA	reverse primer for 5' fragement of m6 mutant
KJ008	KJ TMO7 M7 N-term R	GGCAGCTGCGGCCGCGGCAGCCGCTGCATCTTGTAAC ACCCTGCTG	reverse primer for 5' fragement of m7 mutant
KJ009	KJ TMO7 M8 N-term R	GGCAGCTGCGGCCGCGGCAGCCGCTGCATGCAGATTC CGTATGTAGT	reverse primer for 5' fragement of m8 mutant
KJ010	KJ TMO7 M9 N-term R	GGCAGCTGCGGCCGCGGCAGCCGCTGCCCTCACTTA GATCATCAA	reverse primer for 5' fragement of m9 mutant
KJ011	KJ TMO7 M10 N-term R	GGCAGCTGCGGCCGCGGCAGCCGCTGCGTCTGAGTTT GCTAGTAACT	reverse primer for 5' fragement of m10 mutant
KJ012	KJ TMO7 M11 N-term R	GGCAGCTGCGGCCGCGGCAGCCGCTGCGCTTCTGATT AAAGCAGCTT	reverse primer for 5' fragement of m11 mutant
KJ013	KJ TMO7 M1 C-term F	GCAGCGGCTGCCGCGGCCGCGAGCTGCCTCATCAGGAA CTTCAAGGAT	Forward primer for 3' fragment of m1 mutant
KJ014	KJ TMO7 M2 C-term F	GCAGCGGCTGCCGCGGCCGCGAGCTGCCGATCAAATCA ATGATCTGATTA	Forward primer for 3' fragment of m2 mutant
KJ015	KJ TMO7 M3 C-term F	GCAGCGGCTGCCGCGGCCGCGAGCTGCCTTGCAACAGC TTCTTCTGAG	Forward primer for 3' fragment of m3 mutant
KJ016	KJ TMO7 M4 C-term F	GCAGCGGCTGCCGCGGCCGCGAGCTGCCAGGGACAGTC GTCGTCCGA	Forward primer for 3' fragment of m4 mutant
KJ017	KJ TMO7 M5 C-term F	GCGGCTGCCGCGGCCGCGAGCTGTATGCTGAATCTAACT AAGT	Forward primer for 3' fragment of m5 mutant
KJ018	KJ TMO7 M6 C-term F	GCAGCGGCTGCCGCGGCCGCGAGCTGCCACGTGCAACT ACATACGGAA	Forward primer for 3' fragment of m6 mutant
KJ019	KJ TMO7 M7 C-term F	GCAGCGGCTGCCGCGGCCGCGAGCTGCCAGAGAGGTTG ATGATCTAAG	Forward primer for 3' fragment of m7 mutant
KJ020	KJ TMO7 M8 C-term F	GCAGCGGCTGCCGCGGCCGCGAGCTGCCCTATCTGAGTT ACTAGCAA	Forward primer for 3' fragment of m8 mutant
KJ021	KJ TMO7 M9 C-term F	GCAGCGGCTGCCGCGGCCGCGAGCTGCCACTGCACAAG CTGCTTTAATCAGA	Forward primer for 3' fragment of m9 mutant
KJ022	KJ TMO7 M10 C-term F	GCAGCGGCTGCCGCGGCCGCGAGCTGCCTACTTACCCA ATATCCTTATGA	Forward primer for 3' fragment of m10 mutant
KJ023	KJ TMO7 M11 C-term F	GCAGCGGCTGCCGCGGCCGCGAGCTGCCCTGATTATG CTGGATCCATGGT	Forward primer for 3' fragment of m11 mutant
KJ024	KJ GFP-LIC R	TTATGGAGTTGGGTTCCGAATTACTTGTACAGCTCGTCC A	Reverse primer for amplifying alenine linker mutant
KJ 276	KJ bHLH151 F	TAGTTGGAATGGGTTCCATGGGTGTAACATTAGAAGG	Forward primer for bHLH151
KJ 277	KJ bHLH151 R	AGCATAATCAGGAACATCATAAGGATAAACACAGTTA GTTTCGGTCA	Reverse primer for bHLH151
KJ 278	KJ GFP F	TATCCTTATGATGTTCTGATTATGCTATGGTGAGCAA GGGCGAGGA	Forward primer of GFP for bHLH151/138-GFP
KJ 279	KJ bHLH138 F	TAGTTGGAATGGGTTCCATGGAACGTTACACAAAAA	Forward primer for bHLH138
KJ 280	KJ bHLH138 R	AGCATAATCAGGAACATCATAAGGATAAAAGTGGTGT ACAAATCTAA	Reverse primer for bHLH138
KJ 301	KJ bHLH151M5 5'R	cttgctggaacgacgactgtccctaaacagctcttttagcgtct	Reverse primer for 5' fragment of M5 insertion

KJ 302	KJ bHLH151M5 3'F	aggacagctgctgctccgacaagtagtaggactcttagaca	Forward primer for 3' fragment of M5 insertion
KJ 305	KJ bHLH138M5 5'R	cttgctggaacgacgactgtccctaatgaggtctttaagtcga	Reverse primer for 5' fragment of M5 insertion
KJ 306	KJ bHLH138M5 3'F	aggacagctgctgctccgacaaggaagcatccattgtcaaga	Forward primer for 3' fragment of M5 insertion
KJ 311	KJ bHLH138M89 5'R	taactcagatagctcacttagatcatcaacctctctaactcgttgatgaaacga	Reverse primer for 5' fragment of M8, M9 insertion
KJ 312	KJ bHLH138M89 3'F	ctaagtgagctatctgagttagctagcaaacactgacacaaagactagttagcgagct	Forward primer for 3' fragment of M8, M9 insertion
KJ 313	KJ bHLH151M89 5'R	taactcagatagctcacttagatcatcaacctctctcaagccaagataatactg	Reverse primer for 5' fragment of M8, M9 insertion
KJ 314	KJ bHLH151M89 3'F	ctaagtgagctatctgagttagctagcaaacactgacagcaaatgaaagtgaaagtat	Forward primer for 3' fragment of M8, M9 insertion
KJ 240	KJ LIC-bHLH134 F	TAGTTGGAATGGGTTCCATGTCTTCTAGCAGAAGGTC	Forward primer for bHLH134-GFP
KJ 214	KJ bHLH134 R	TCCTCGCCCTTGCTCACCATTCATTAATCAAGCTCCTAA	Reverse primer for bHLH134-GFP
KJ 241	KJ LIC-bHLH136 F	TAGTTGGAATGGGTTCCATGTGCAACAGAAGATCAAGG	Forward primer for bHLH136-GFP
KJ 216	KJ bHLH136 R	TCCTCGCCCTTGCTCACCATCATGAGTAGGCTTCTAATAA	Reverse primer for bHLH136-GFP
KJ 233	KJ LIC-bHLH161	TAGTTGGAATGGGTTCCATGGCGACGAACATCGGAAT	Forward primer for bHLH161-GFP
KJ145	KJ bHLH161 R	tcctcgccctgctcaccatctgcataagcaaacctcgga	Reverse primer for bHLH161-GFP
KJ 242	KJ LIC-bHLH166 F	TAGTTGGAATGGGTTCCATGTCTAACAGAAGATCAAG	Forward primer for bHLH166-GFP
KJ 219	KJ bHLH166 R	TCCTCGCCCTTGCTCACCATCATGAGTAAGCTTCTAATCA	Reverse primer for bHLH166-GFP
KJ 229	KJ LIC-NES-GFP R	TTATGGAGTTGGGTTTCATCAAGAGTAAGTCTTTCAAGAGGAGGAAGTTGAAGCTTGTACAGCTCGTCCATGC	Reverse primer for TMO7-GFP-NES
KJ 231	KJ LIC-NLS-TMO7 F	TAGTTGGAATGGGTTCCATGCCTAAGAAGAAGAGGAAAGTTATGTCGGGAAGAAGATCACG	Forward primer for NLS-TMO7-GFP
KJ 281	KJ TMO7 S39A 5' R	cttgctggaacgacgagcgtccct	Reverse primer for TMO7S39A 5' fragmen
KJ 282	KJ TMO7 S42A 5' R	cttgctggaacgacgagcgtccct	Reverse primer for TMO7S42A 5' fragment
KJ 283	KJ TMO7 S39A 3' F	aggacagctgctgctccgacaag	Forward primer for TMO7S39A 3' fragment
KJ 284	KJ TMO7 S42A 3' F	aggacagctgctgctccgacaag	Forward primer for TMO7S42A 3' fragment
KJ 249	KJ TMO7 CRISPR amplify F	ATTTTTCATAAAACAAATAAT	Forward primer for amplifying TMO7 genomic fragment for genotyping
KJ 250	KJ TMO7 CRISPR amplify R	CCTCTCTATGCAGATTCCGT	Reverse primer for amplifying TMO7 genomic fragment for genotyping
KJ 251	KJ TMO7 CRISPR sequencing F	acataataacaaccgtcact	sequencing primer for genotyping CRISPR/Cas9 tmo7
KJ526	KJ qbHLH134 F	GAACAAGGAAGCCGATGACC	qPCR primer for bHLH134
KJ527	KJ qbHLH134 R	GCTCCTAATAACTGCGGCTTG	qPCR primer for bHLH134
KJ530	KJ qbHLH136 F	GCATCAGCCTCGAAAGTATTGC	qPCR primer for bHLH136
KJ531	KJ qbHLH136 R	AAACGCTCGCTCAGATTGTC	qPCR primer for bHLH136
KJ534	KJ qbHLH161 F	AAGGAACCTGAGCAAAGAAGTGG	qPCR primer for bHLH161
KJ535	KJ qbHLH161 R	TTCGGATTAGTGCAGCTTGAG	qPCR primer for bHLH161
KJ538	KJ qbHLH166 F	TGTCAGCATCAAAGGTAACAAGA	qPCR primer for bHLH166
KJ539	KJ qbHLH166 R	TCAAGAAGCTGCGACAAACG	qPCR primer for bHLH166
BR210	Q_TMO7_end_F	CAACTACATACGGAATCT	qPCR primer for TMO7
BR211	Q_TMO7_end_R	AAGATAGATAGGAATTATTGG	qPCR primer for TMO7
JP001	ACT2	CTCCATTGTTTGTTCATT	qPCR primer for ACT2
JP002	ACT2	TCAATTCGATCACTCAGA	qPCR primer for ACT2
U6-F-Slice		ttactagataactagctgctgcccgc TCGTTGAACAACGGAAACTCG	Forward primer for U6 promoter amplification with adaptor site for SLICE

TMO7 -U6- sg-R		TGTCGGAACGACGACTGTCCAATCACTACTTCGACTC TAG	Reverse primer with TMO7 sgRNA site to amplify U6 promoter
TMO7 -guide- F		GGACAGTCGTCGTTCCGACAGTTTATAGAGCTAGAAAT AGC	Forward primer with TMO7 sgRNA site to amplify sgRNA scaffold
guide- R-Slice		gcttgagctctcccatatggtcgaccGAATTCGAGCTCGGTACCC	Reverse primer for sgRNA scaffold amplification with adaptor site for SLiCE

Table S2. Two of the predicted phosphorylation sites are located in M5 region.

http://www.dabi.temple.edu/disphos/				
DISPHOS Results				
Position	Residue	Score	Sequence	Yes/No
2	S	0.987	***MSGRRS	YES
6	S	0.984	SGRRRSRQ	YES
8	S	0.94	RRRSRQSS	YES
11	S	0.813	RSRQSSGTS	YES
12	S	0.682	SRQSSGTSR	YES
14	T	0.02	QSSGTSRIS	
15	S	0.691	SSGTSRISE	YES
18	S	0.479	TSRISEDQI	
39	S	0.751	ELR DSRRSD	YES
42	S	0.64	DSRRSDKVS	YES
46	S	0.295	SDKVSAARV	
54	T	0.006	VLQDTCNYI	
57	Y	0.02	DTCNYIRNL	
69	S	0.341	VDDLSERLS	
73	S	0.411	SERLSELLA	
79	S	0.141	LLANSDTAQ	
81	T	0.042	ANSDTAQAA	
89	S	0.13	ALIRSLLTQ	
92	T	0.006	RSLLTQ***	

Table S3. *tmo7-4*, -5 and -6 have significantly shorter root compare to Col.

	Length		Length		Length		Length
Col	2.69	<i>tmo7-4</i>	1.814	<i>tmo7-5</i>	1.885	<i>tmo7-6</i>	2.046
	2.645		1.812		1.74		1.683
	2.398		1.773		1.56		1.679
	2.393		1.731		1.543		1.612
	2.358		1.71		1.531		1.5
	2.333		1.703		1.487		1.491
	2.311		1.663		1.465		1.481
	2.228		1.602		1.463		1.472
	2.164		1.599		1.431		1.472
	2.137		1.584		1.369		1.461
	2.114		1.581		1.358		1.438
	2.093		1.531		1.29		1.344
	2.065		1.469		1.244		1.279
	1.897		1.428		1.209		1.203
	1.848		1.397		1.207		1.165
	1.77		1.367		1.165		1.159
	1.753		1.355		1.136		1.155
			1.298		1.093		1.026
			1.244		1.033		0.888
			0.952				
p-value		<i>tmo7-4</i>	1.59408E-09	<i>tmo7-5</i>	2.24588E-11	<i>tmo7-6</i>	3.38143E-10

Table S4 pTMO7::TMO7-GFP rescued the *tmo7* embryo phenotype.

Line	mutant number	wild type number	Total number	%
Col	5	217	222	2.25
<i>tmo7-4</i>	15	163	178	8.43
pTMO7::TMO7-GFP T2-1	5	216	221	2.26
pTMO7::TMO7-GFP T2-2	2	141	143	1.40
<i>tmo7-5</i>	9	127	136	6.62
pTMO7::TMO7-GFP T2-1	6	267	273	2.20
pTMO7::TMO7-GFP T2-2	5	228	233	2.15
pTMO7::TMO7-3GFP T2-1	3	188	191	1.57
<i>tmo7-6</i>	9	198	207	4.35
pTMO7::TMO7-GFP T2-2	2	144	146	1.37
pTMO7::TMO7-3GFP T2-2	9	197	206	4.37
pTMO7::TMO7-3GFP T2-3	11	252	263	4.18
pTMO7::TMO7-3GFP T2-5	14	224	238	5.88

Table S5. p*TMO7*::TMO7-GFP did not rescue the *cald3-2d* hypophysis phenotype

Lines in <i>cals3-2d</i>	mutant number	wild type number	Total number	%
p <i>TMO7</i> ::TMO7-GFP T3-10-2	189	3	192	1.56
p <i>TMO7</i> ::TMO7-GFP T3-15-5	220	2	222	0.90
p <i>TMO7</i> ::TMO7-GFP T3-15-9	193	3	196	1.53
pDR5::GFP T3-3-4	190	2	192	1.04
pDR5::GFP T3-10-1	143	2	145	1.38
pDR5::GFP T3-11-7	167	2	169	1.18